

CZECH TECHNICAL UNIVERSITY IN PRAGUE

FACULTY OF MECHANICAL ENGINEERING

Bc. Martin Havránek

**PATOBIO MECHANICS OF FOREARM IN
PROPERATIVE PLANNING**

DIPLOMA THESIS

**PATOBIO MECHANIKA PŘEDLOKTÍ PŘI
PŘEDOPERAČNÍM PLÁNOVÁNÍ**

DIPLOMOVÁ PRÁCE

2022

I. OSOBNÍ A STUDIJNÍ ÚDAJE

Příjmení: **Havránek** Jméno: **Martin** Osobní číslo: **473637**
Fakulta/ústav: **Fakulta strojní**
Zadávací katedra/ústav: **Ústav mechaniky, biomechaniky a mechatroniky**
Studijní program: **Aplikované vědy ve strojním inženýrství**
Specializace: **Biomechanika**

II. ÚDAJE K DIPLOMOVÉ PRÁCI

Název diplomové práce:

Patobiomechanika předloktí při předoperačním plánování

Název diplomové práce anglicky:

Pathobiomechanics of forearm in preoperative planning

Pokyny pro vypracování:

1. Biomechanika předloktí - funkce jednotlivých kloubů
2. Vytvoření 3D modelu geometrie kostí
3. Definice zlomeniny a malunionu
4. Model kinematiky normálního a nemocného předloktí
5. Predikce rozsahu pohybu předloktí v pronaci a supinaci
6. Aplikace modelu v klinické kazuistice

Seznam doporučené literatury:

Padmore CE, Stoesser H, Nishiwaki M, Gammon B, Langohr GDG, Lalone EA, Johnson JA, King GJW. The Effect of Dorsally Angulated Distal Radius Deformities on Carpal Kinematics: An In Vitro Biomechanical Study. J Hand Surg Am. 2018 Nov;43(11):1036.e1-1036.e8. doi: 10.1016/j.jhssa.2018.02.017.
Carrillo F, Roner S, von Atzigen M, Schweizer A, Nagy L, Vlachopoulos L, Snedeker JG, Fűrnstahl P. An automatic genetic algorithm framework for the optimization of three-dimensional surgical plans of forearm corrective osteotomies. Med Image Anal. 2020 Feb;60:101598. doi: 10.1016/j.media.2019.101598.

Jméno a pracoviště vedoucí(ho) diplomové práce:

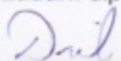
prof. RNDr. Matej Daniel, Ph.D. České vysoké učení technické v Praze, Fakulta strojní

Jméno a pracoviště druhé(ho) vedoucí(ho) nebo konzultanta(ky) diplomové práce:

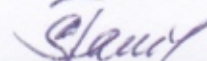
Datum zadání diplomové práce: **19.04.2022**

Termín odevzdání diplomové práce: **14.08.2022**

Platnost zadání diplomové práce:


prof. RNDr. Matej Daniel, Ph.D.
podpis vedoucí(ho) práce

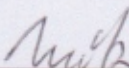

doc. Ing. Miroslav Španiel, CSc.
podpis vedoucí(ho) ústavu/katedry


doc. Ing. Miroslav Španiel, CSc.
podpis děkana(ky)

III. PŘEVZETÍ ZADÁNÍ

Diplomant bere na vědomí, že je povinen vypracovat diplomovou práci samostatně, bez cizí pomoci, s výjimkou poskytnutých konzultací. Seznam použité literatury, jiných pramenů a jmen konzultantů je třeba uvést v diplomové práci.

28.4.2022
Datum převzetí zadání


Podpis studenta

ACKNOWLEDGMENT

Firstly, I would like to thank to prof. RNDr. Matej Daniel Ph. D., my supervisor of my thesis for criticism and valuable advices in regular consultations. Next gratitude belongs to MUDr. Radek Kebrle for consulting and advises from the field of clinical praxis. Without his clinical knowledge and interest in this topic would not this thesis exist.

And finally, I would like to thank my family for their support throughout my studies.

PRONOUNCEMENT

I declare that I have worked out the presented thesis individually and that I have listed all the information sources used in accordance with the Methodical Instruction on the Ethical Preparation of University Final Theses.

Place: Kladno.....

Date: 9.8.2022.....



.....
Signature

ABSTRACT

The subject of the diploma thesis is the pathobiomechanics of forearm in preoperative planning. Brief description of musculoskeletal anatomy of a forearm is provided. State of the art of forearm surgery, dealing with malunions and biomechanics of the forearm during the healthy and pathological rotation is discussed in details. New approach to modelling of pro/supination movement is proposed. The various models of pathological factors effecting the malunited rotation are formulated. It could be done an original 3D model for a specific patient. The pathological rotation could be adjusted for individual person specific stiffness of ligaments and soft tissues. The forearm pathological kinematics with effect of soft tissues, ligament and dynamic centre of rotation is explicitly included on the contrary to current preoperative softwares. The novel modelling approach was verified by comparison to the clinical data.

ABSTRAKT

Předmětem diplomové práce je patobiomechanika předloktí v předoperačním plánování. Je uveden stručný popis muskuloskeletální anatomie předloktí. Podrobně je diskutován současný stav chirurgie předloktí, zabývající se maluniony a biomechanikou předloktí při zdravé a patologické rotaci. Je navržen nový přístup k modelování pro/supinačního pohybu. Jsou formulovány různé modely patologických faktorů ovlivňujících narušenou rotaci. Může být vytvořen originální 3D model předloketních kostí pro konkrétního pacienta. Patologická rotace může být upravena pro individuální specifickou tuhost vazů a měkkých tkání. Na rozdíl od současných předoperačních softwarů je explicitně zahrnuta patologická kinematika předloktí s efektem měkkých tkání, vaziva a dynamického centra rotace. Nový přístup pro modelování 3D kinematiky předloktí byl ověřen srovnáním s klinickými daty.

KEYWORDS

3D preoperative planning, Forearm surgery, STL reconstruction from CT scans, Forearm kinematics, Malunions, Range of motion, Patobiomechanics, Angulation

KLÍČOVÁ SLOVA

3D předoperační plánování, Chirurgie předloktí, STL rekonstrukce z CT snímků, Kinematika předloktí, Malunion, Rozsah pohybu, Patobiomechanika, Angulace

TABLE OF CONTENTS

LIST OF USED ABBREVIATIONS.....	5
LIST OF USED SYMBOLS.....	6
INTRODUCTION.....	7
1. FUNCTIONAL ANATOMY OF FOREARM.....	8
1.1. ELBOW.....	8
1.2. PROXIMAL RADIOULNAR JOINT.....	9
1.3. INTEROSSEOUS MEMBRANE.....	9
1.4. DISTAL RADIOULNAR JOINT.....	10
1.5. MUSCULAR SYSTEM.....	10
2. STATE OF THE ART.....	11
3. AIM OF THE WORK.....	16
4. METHODS.....	17
4.1. DATA PREPARATION.....	17
4.2. STL SURFACE INTERSECTION.....	21
4.3. MODELING OF NORMAL ROTATION.....	22
4.3.1. ONE AXIS ROTATION.....	22
4.3.2. DYNAMIC CENTRE OF ROTATION.....	24
4.4. MALUNION MODELING.....	28
4.5. MODELING OF PATHOLOGICAL ROTATION.....	31
4.5.1. ROTATION CENTRE TRANSLATION BY ANGULATION.....	31
4.5.2. ROTATION IN RADIOHUMERAL JUNCTION.....	33
4.5.3. MODEL SET UP BY STIFFNESS PARAMETRES.....	34
4.5.4. LONGITUDIANAL RADIUS TRANSLATION.....	37
4.6. CLINICAL PROCESS OF 3D PREOPERATIVE KINEMATICS PLANNING.....	38
5. RESULTS.....	42
5.1. NORMAL ROTATION.....	42
5.2. PATHOLOGICAL ROTATION.....	43
5.2.1. KINEMATICS OF FREE ROTATION.....	43
5.2.2. KINEMATICS –ROTATION CENTRE TRANSLATION.....	44
5.2.3. KINEMATICS – RADIOHUMERAL ROTATION.....	46
5.2.4. KINEMATICS – EFFECT OF STIFFNESS PARAMETRES.....	47
5.2.5. KINEMATICAL MODEL VERIFICATION.....	50
5.2.6. CLINICAL DATA EVALUATION.....	52
6. DISCUSSION.....	55
CONCLUSIONS.....	57
REFERENCES.....	58
LIST OF FIGURES.....	61
LIST OF TABLES.....	63

LIST OF USED ABBREVIATIONS

CF	Cost function
CT	Computed tomography
DICOM	Digital Imaging and Communications in Medicine
DRUJ	Distal radioulnar joint
HU	Hounsfield Unit
IOM	Interosseus membrane
LB	Lower bound
Lig.	Ligamentum
MDRF	Malunion of distal radius
MRI	Magnetic resonance imaging
PRUJ	Proximal radioulnar joint
ROI	Range of interest
ROM	Range of motion
SA	Simulated Annealing
SD	Standard deviation
STL	Standard Tessellation Language
TFCC	Triangular fibrocartilage complex
UB	Upper bound

LIST OF USED SYMBOLS

\vec{r}	vector
$\vec{\vec{R}}$	tensor
\vec{r}^T	transposition of a vector
$\vec{\vec{R}}^T$	transposition of a tensor
\vec{I}	identity matrix
$\overrightarrow{r_{idn}}$	i-th transformation of the n-th vector from the distal part of STL file
$inv(\vec{\vec{R}})$	inversion of a tensor
$\vec{e}_1 \times \vec{q}$	cross product
$\vec{e}_1 \otimes \vec{e}_1^T$	Kronecker product
$\vec{V} \cdot \overrightarrow{nFABC}$	dot product
α [°]	rotation incremental angle
β [°]	angle between frontal plane and angulation plane
δ [°]	angle between the axis of angulated distal radius and proximal radius
φ, β_r [°]	angle of volar/dorsal angulation
ϵ, α_r [°]	angle of medial angulation
π [°]	angle of distal radius axial rotation
θ [°]	angle of ventro – dorsal rotation in radiohumeral junction
ξ [°]	angle of medio – lateral rotation in radiohumeral junction
F [N]	force generated by IOM
k_{IOM} [N/m]	stiffness of IOM
l_0 [m]	initial length of IOM
l [m]	length of IOM in the deformed state
k [J/K]	Boltzmann constant (1.380649*10 ⁻²³ J/K)

INTRODUCTION

Nowadays, the 3D preoperative planning is starting to be used widely in the orthopedy. The operator has an advantage to do the surgery in the virtual environment and plan precisely how to proceed during the surgery. This planning is especially important in the forearm surgery. Recently a functional view comes to the fore, which considers the entire forearm as one unit forming v essentially the largest joint in the human body [1]. From a biomechanical point of view, this is a closed kinematic chain. It means that the failure of each part of the forearm is never isolated and leads to a malfunction of the forearm as a whole and therefore to the restriction of the rotation of the hand and to the disruption of the normal transmission of forces. [2]. It was proved that even a relatively small impairment of forearm function is perceived by the patient as significant reduced quality of life [3]. In terms of forearm trauma, the most common traumatic injury to the forearm is a fracture. Forearm fractures can be treated conservatively or surgically. Conservative treatment consists in closed fracture reduction and subsequent immobilization using plaster or plastic fixation bandage. The surgical solution includes methods from the least invasive to open osteosynthesis. The surgical solution is usually preceded by 3D visualization in the preoperative planning software.

Currently available softwares don't allow to simulate post operative precise kinematics including all significant structures that affecting the rotation. The ROM is influenced by many factors one of them is a specific geometry of patient's bones articulating surfaces. Therefore, a kinematics simulation is needed for each patient. Sometimes it happens that the bone after an operation doesn't health in the proper shape and malunion occurs. In the case of vast majority of bones in human body it doesn't influence the kinematics significantly. But in the case of forearm the kinematics of pronation and supination is very sensitive to small deformities, this sensitivity could lead to serious limitation of ROM. Because there are many factors that are influencing the pathological rotation of a forearm. Forearm assumed as one joint is the most complex joint in the human body in terms of kinematics. That's the reason for precise kinematical study of this joint.

The attention is devoted to the precise kinematics simulation of pro/supination movement of normal and pathological forearm. 3D visualization, that is developed in this thesis, can be used in 3D preoperative software to determine ROM if a small surgical imperfection occurs. Based on this study it is possible to decide whether to use precise 3D printed custom splints or conventional procedure.

1. FUNCTIONAL ANATOMY OF FOREARM

Functional anatomy of forearm gives us an instrument how to understand forearm as a mechanism. The specific organization and form of forearm structures follows their function. Therefore, if some disorder or imperfection concerning the form of a structure occurs, then it could have significant consequences on kinematics of hand. The main function of upper limb is to make a precise 3D movement of a hand, that could be imaged as an end effector of an open kinematic chain mechanism. Elbow and forearm are responsible for a movement in two axes of rotation.

We devoted attention to the anatomy and function of crucial structures of forearm responsible for controlled pro/supination. Therefore, the muscle system of forearm is not described in detail because only 3 muscles are responsible for pro/supination movement.

In this thesis just the bone kinematics is solved without adding the dynamic of muscles. That is an additional reason for the short description of forearm muscular system.

1.1. ELBOW

The elbow could be defined as proximal end of the forearm (antebrachium). Elbow joint (Articulatio cubiti) contains three bones: humerus, ulna, and radius. This articulation can be divided into three independent articulations (Articulatio humeroulnaris, Articulatio humeroradialis, Articulatio radioulnaris proximalis). The distal humerus consists of two condyles making articular surfaces of the capitellum humeri laterally and trochlea humeri medially. [4] Trochlea humeri is an attachment for incisura trochlearis ulnae, that is the articular surface on ulna. Together they are forming Articulatio humeroulnaris (hinge joint). This articulation stands for rotation around the axis which is approximately perpendicular to the axis of humerus and ulna. These movements are called flexion and extension. The significant structures on humerus are required: the coronoid and radial fossa for full range of motion during the flexion of forearm anteriorly. Coronoid fossa enables to place coronoid process on ulna and radial fossa makes placement for radial head. Olecranon fossa is necessary for olecranon process placement on ulna during extension from the posterior side. [4]

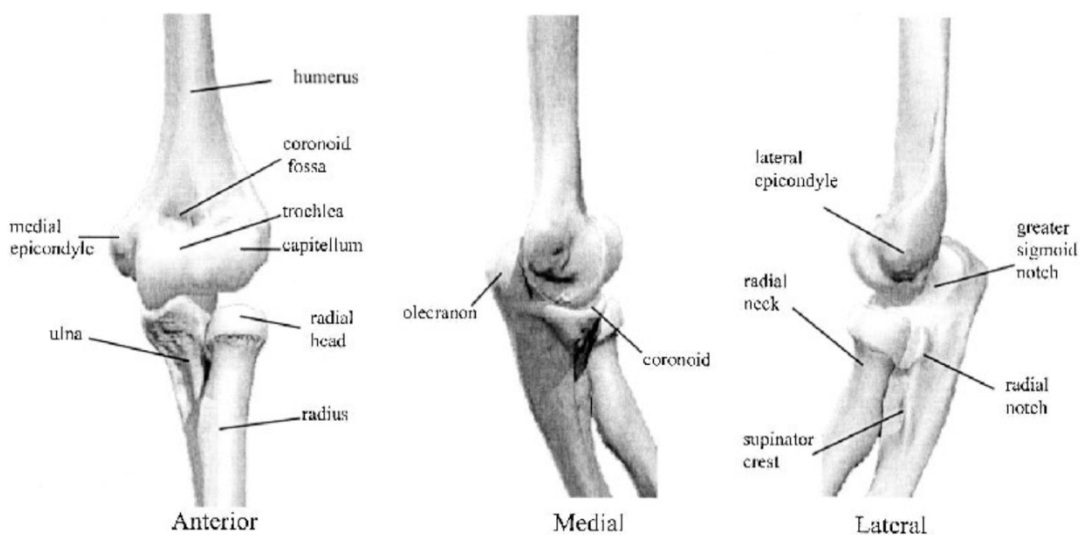


Fig. 1 – The elbow joint [4]

Elbow ligaments have stabilizing function. The elbow joint is stabilized from medial and lateral side by ligamentum collaterale ulnare and ligamentum collaterale radiale respectively. Lig. collaterale ulnare from the medial side has a triangular shape formed by three parts. [5]

1.2. PROXIMAL RADIOULNAR JOINT

Proximal head of radius (caput radii) forms two articulations responsible for rotation around a specific axis with ulna and humerus. From lateral side of ulna there is a radial notch (incisura radialis) which makes together with the radial head Articulatio radioulnaris proximalis – PRUJ (pivot joint). Head of radius with capitulum humeri form together Articulatio humeroradialis (spheroid joint). The irregular shape of articular flats of PRUJ is cause of ulna contra – rotation in a small range. This contra – rotation has effect on lesser range of pronation and bigger range of supination during elbow flexion and on low range of supination and large range of pronation during elbow extension. [6]

Lig. anulare radii clamps on ulna and wraps around the radius to prevent lateral dislocation. Annular ligament also due to synovial membrane reduces friction during rotation due to synovial membrane. [5]

1.3. INTEROSSEOUS MEMBRANE

There is membrane interossei between radius and ulna. This membrane is a connective tissue that serves to hold forearm bones together during pronation and supination and also transfer forces from radius to ulna. [5] It provides stability to the DRUJ and the longitudinal stability for the forearm. IOM prevents longitudinal translation. It also serves as an origin for forearm musculature. [8]

IOM is composed of five single components: a central band, a distal oblique bundle, an accessory band, a dorsal oblique accessory cord, and a proximal oblique cord. [8] IOM can be understood as a tensegrity structure because all ligaments of IOM are effectively orientated to transfer just a tension.

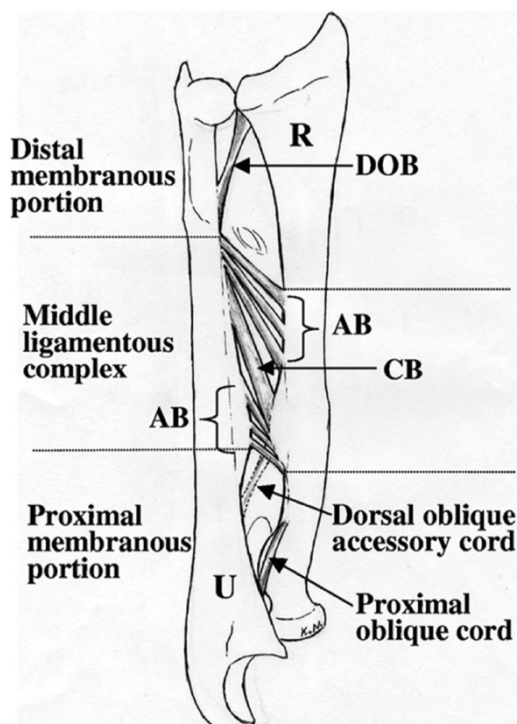


Fig. 2 – Interosseous membrane [8]

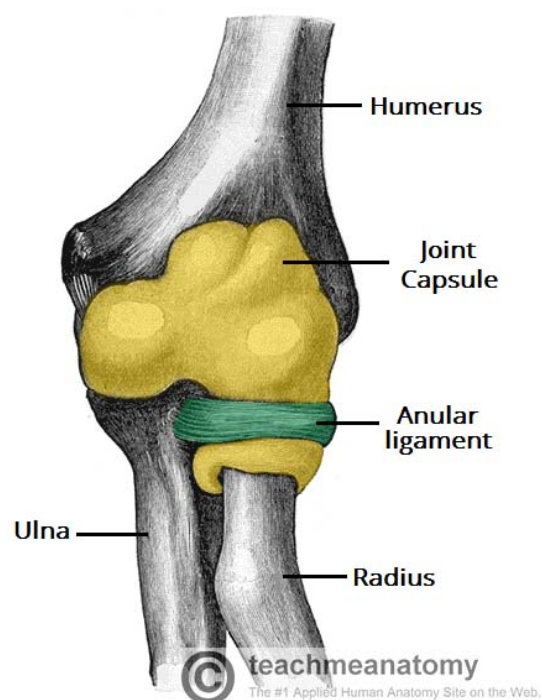


Fig. 3 – PRUJ, ligamentum anulare [5]

1.4. DISTAL RADIOULNAR JOINT

Distal radioulnar joint could be defined as distal end of the forearm. DRUJ is comprised of articular surfaces of distal ends of ulna and radius. *Articulatio radioulnaris distalis* connects together structures *incisura ulnaris* on radius and *circumferentia articularis* on ulna. DRUJ is defined as a pivot joint and it is connected by the same axis of rotation with PRUJ. There are anterior and posterior ligaments to strengthen the joint and in addition there is an articular disk. This articular disk is responsible for binding radius and ulna within the rotation and for separating DRUJ from the wrist. [5] TFCC is an anatomical strong fibrocartilage structure composed of five parts: the articular disc, the superficial and deep radioulnar fibers, and the two disc-carpal ligaments. It is stretched between ulna and radius at the end of DRUJ. The stabilization of DRUJ is provided by the joint capsule TFCC and the capsule surrounding structures. [7]

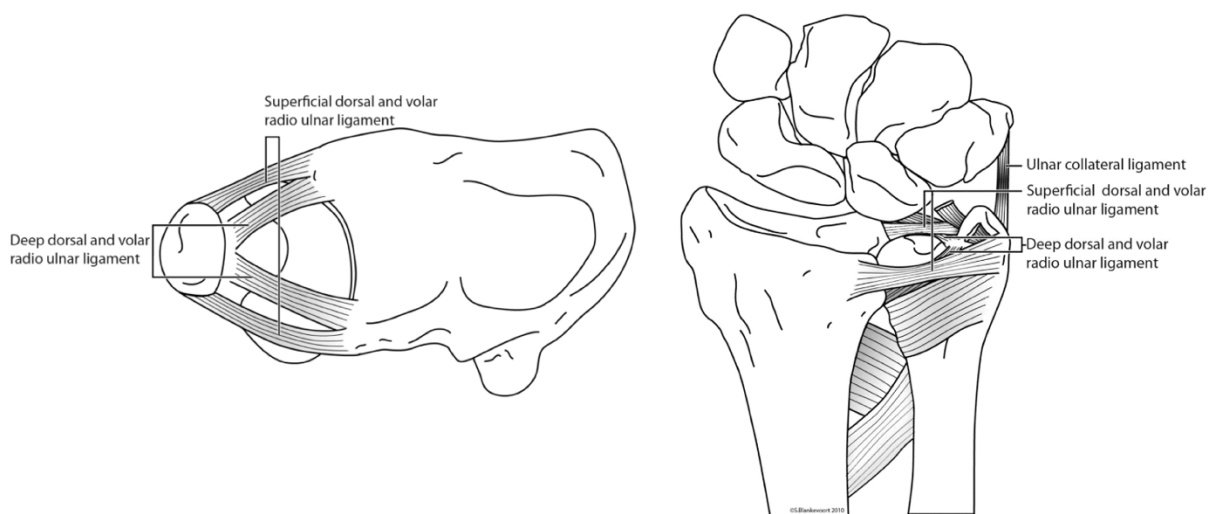


Fig. 4 – DRUJ, TFCC [7]

1.5. MUSCULAR SYSTEM

Muscular system of forearm consists of twenty muscles. The muscles can be divided into the two compartments: the anterior and the posterior. Each compartment is divided into a superficial and a deep group of muscles. The function of the anterior group of muscles is flexion of hand and fingers. The posterior group stands for extension of hand and fingers. [9]

Superficial layer of flexors includes the pronator teres that is responsible for pronation. The attachment site for pronator teres is the middle portion of the radius. In the deep compartment of flexors, we find another pronator, pronator quadratus. It originates on the distal anteromedial ulna and inserts on the distal anterolateral radius. Musculus supinator which starts on the lateral epicondyle of the humerus is located in the posterior compartment. Supinator is wrapping around the back of the arm and connects to the radius at the same location as at pronator teres. Musculus supinator is responsible for the supination of the forearm. [9]

2. STATE OF THE ART

This chapter includes abstracts from peer-reviewed articles on forearm surgery and forearm biomechanics. It will show the current situation and knowledge about these topics.

DISTAL RADIUS MALUNION [10]

DOI: <https://doi.org/10.1016/j.jhsa.2020.02.008>

The fractures that appear on the distal end of radius are common injuries comprising 12% to 17% of all fractures. These fractures are very often followed by the malunion of distal radius fractures (MDRF). If the fracture is treated with cast immobilization, MDRF appeared historically in 24% of cases. The incidence of MDRF with the usage of advanced surgical techniques is 11%.

MDRF results in a fundamental in the biomechanics of wrist. Among the complications we can find limited mobility, arthritis, dysfunction, change of the direction of the flexor tendons due to decreased radial inclination, this phenomenon leads to decreased mechanical advantage. Last not least is the effect at the distal radioulnar joint (DRUJ). The axis of rotation can alter, that leads to limited forearm pronation and supination. Moreover, strain on the triangular fibrocartilage complex (TFCC) can occur and can lead to tearing. Another consequence can be radial shortening that is associated with a shift of force transfer from the radiocarpal to ulnocarpal joint. The shortening of 2.5 cm of radius increases the force in the ulnocarpal joint by 42%. Bronstein and colleagues found that 10 mm of loss of radial height results in loss of supination (29%) and pronation (47%).

For the preoperative preparations are used 3D Guides. Kunz et al described this technique and their experience in 9 patients with a distal radius malunion with an average follow-up of 7 months. The average deviation between the achieved and planned radial inclination in these patients was 1.8° (SD, 0.8°); for volar tilt, 1.9° (SD, 1.5°); and for ulnar variance, 0.9 mm (SD, 1.1 mm). The authors identified 2 complications: one infection and one case of posttraumatic arthrosis that required a wrist arthrodesis.

NEAR – ANATOMICAL CORRECTION USING A CT – GUIDED TECHNIQUE OF A FOREARM OF A FOREARM MALUNION IN A 15-YEAR-OLD GIRL: A CASE REPORT INCLUDING SURGICAL TECHNIQUE [11]

DOI: <https://doi.org/10.1016/j.otsr.2017.03.017>

Forearm fractures are the most common fracture in childhood. The incidence is between 3.4% to 13% of all pediatric fractures. Seventy percent of the surgeries in forearm fractures, are performed due to occurrence of malunion and subsequent dysfunction following conservative treatments. The article describes the postoperative trauma of a patient that has the angulation of radius 11.9° in coronal plane, 11.3° in sagittal plane and axial rotation was 3.96°. The ulna angulation was observed with coronal bowing 5.5°, sagittal bowing 9.6° and axial rotation 22.9°. This led to the restriction of supination to 10 degrees of motion while the pronation was maintained. The corrective osteotomy is needed in this case. The closing wedge osteotomy of 3.2 mm correcting the radius in 3 planes was performed.

Six months after surgery a postoperative CT scan of both arms was performed to analyze ultimate correction. Compared to the planned correction the ulna was corrected in the coronal, sagittal and axial plane with respectively 0.3°, 0.5° and 0.1° accuracy. The radius was corrected

with 4.9°, 0.6° and 1.38° accuracy for the coronal, sagittal and axial plane. The full functional capacity was regained.

CORRECTION OF FOREARM MALUNION GUIDED BY PREOPERATIVE COMPLAINT [12]

DOI: 10.1007/s11999-008-0234-3

Forearm malunions are responsible for impairment in ROM through different mechanisms. The angular deformities of forearm bones produce tension in the interosseous membrane and bone collision that disables free rotation of the radius around forearm axis of rotation. In the experiment were 3 groups of people. Group 1 had predominant loss of pronation. Group 2 had predominant loss of supination. Group 3 had a painful DRUJ without any movement difficulties. 72% of malunions were found in the middle third of radius and 90% in the middle third of ulna. In Group 1, all malunions were located in the proximal two-thirds of the radius and the ulna with both forearm bones always involved with angular deformities. Four patients in this group also had axial malunions of 30° or greater affecting one of the forearm bones. In Group 2, all but one patient had combined angular malunions of the radius and ulna. No patient in this group had a rotational malunion of the radius of 30° or greater, and only one patient (Patient 8) had a combined rotational malunion of the ulna equal to 25°. Conversely, all but one patient (Patient 11) in Group 3 had an isolated malunion of the radius. All patients in this group had malunions of the radius located in the distal half of the bone, six of seven were in the distal third.

Group	Patient number	Pronation/supination (degrees)			ROM difference (degrees)		Assessment at last followup	
		Injured side preoperatively	Injured side postoperatively	Healthy side	Postoperatively-preoperatively	Postoperatively-healthy side	Relative grip strength (%)	DASH score
1	1	15-0-75	50-0-20	70-0-80	-20	-80	112%	9
	2	0-10-85	40-0-65	70-0-95	30	-60	81%	25
	3	10-0-75	60-0-80	65-0-90	55	-15	89%	ND
	4	5-0-90	50-0-90	80-0-80	45	-20	76%	ND
	5	40-0-60	65-0-50	75-0-90	15	-50	74%	30
	6	20-0-70	40-0-80	75-0-85	30	-40	103%	13
2	7	45-0-10	55-0-80	55-0-85	80	-5	83%	37
	8	70-0-0	60-0-90	65-0-90	80	-5	92%	1
	9	90-0-10	80-0-90	90-0-90	70	-10	97%	0
	10	60-10-0	25-0-70	75-0-70	45	-50	109%	3
3	11	70-0-100	75-0-95	85-0-110	0	-25	105%	1
	12	70-0-95	70-0-95	70-0-95	0	0	96%	0
	13	75-0-70	90-0-90	70-0-90	35	-20	91%	3
	14	65-0-100	65-0-120	50-0-120	20	15	72%	17
	15	65-0-80	75-0-90	75-0-90	20	0	93%	7
	16*	50-0-80	55-0-75	55-0-85	0	-10	91%	1
	17	80-0-90	80-0-120	80-0-120	30	0	120%	0

* Double-level-osteotomy; ROM = range of motion; DASH = Disabilities of the Arm, Shoulder and Hand; ND = not determined.

Fig. 5 – ROM investigation in the case of patients with forearm malunion [12]

The type of preoperative complaint defined groups of patients with different potential for improvement in overall ROM after osteotomy. Patients in Group 1 gained $38^\circ \pm 13^\circ$ pronation ($p \setminus 0.001$) but lost $6^\circ \pm 28^\circ$ supination ($p = 0.63$) on average. Patients in Group 2 gained $80^\circ \pm 8^\circ$ supination ($p \setminus 0.0005$) but lost $11^\circ \pm 18^\circ$ pro- nation ($p = 0.31$). All patients in Group 3 gained a stable and pain-free DRUJ, and their ROM statistically was unchanged ($5^\circ \pm 6^\circ$ gain in pronation [$p = 0.06$], $10^\circ \pm 14^\circ$ gain in supination [$p = 0.10$]). The overall ROM (pronation

+ supination) was improved by $29^{\circ} \pm 20^{\circ}$ in Group 1, $69^{\circ} \pm 17^{\circ}$ in Group 2, and $15^{\circ} \pm 15^{\circ}$ in Group 3. The improvement in ROM was greater ($p < 0.002$) in Group 2 than in Group 1. Among the five patients with residual impairment of ROM greater than 30° with respect to the healthy side, four were in Group 1 and one was in Group 2; none was in Group 3. Angulation of 10° of one forearm bone has little impact on motion, but combined deformities of 10° of the radius and ulna toward the interosseous membrane considerably decreases supination but not pronation. Conversely, isolated 20° angulation of the radius reduces pronation in dorsal angulation and supination in volar angulation, and the same angulation toward the interosseous membrane decreases supination and pronation. Combined angular deformities of the radius and ulna in different directions reduce substantially more ROM than combined angulation in the same direction. Proximal deformities had less impact on ROM than equivalent deformities produced at the middle or the distal third of the radius. Isolated axial malunion of the radius in supination markedly reduced pronation but did not change supination, and malunion of the radius in pronation reduced supination but did not change pronation.

THE EFFECT OF DORSAL ANGULATION ON DISTAL RADIOULNAR JOINT ARTHROKINEMATICS MEASURED USING INTERCARTILAGE DISTANCE [13]

DOI: [10.1055/s-0038-1667303](https://doi.org/10.1055/s-0038-1667303)

The most common type of fracture of upper extremity in USA is distal radius fracture. Factors such as osteopenia, comminution, age over 60 years, and a high degree of initial displacement may predispose these to malunion. Malunion are followed by mechanisms such as displaced axis of rotation or change of moment arms of wrist muscles due to dorsal angulation. Malunions in the distal part of radius are causing DRUJ instability and abnormal load transfer across the joint. To the malunion there could be additional effect of torn TFCC. Forearm angulation had a significant effect on contact area ($p = 0.004$), with measurements being highest between 10 and 30 degrees of supination. TFCC sectioning caused a significant decrease in contact area in the DRUJ ($p = 0.030$). Simulated TFCC rupture reduces the DRUJ contact area and significantly increases the variability of the contact centroid pathway during forearm rotation.

THE ROLE OF THE INTEROSSEOUS MEMBRANE AND TRIANGULAR FIBROCARILAGE COMPLEX IN FOREARM STABILITY [14]

DOI: [https://doi.org/10.1016/0363-5023\(94\)90050-7](https://doi.org/10.1016/0363-5023(94)90050-7)

Compressive forces applied on the forearm bones during a fall on the outstretched hand causes bony fractures and soft tissues injuries. Forearm bones and the structures connecting these bones have crucial role in the force transmission from the hand to the elbow. TFCC and IOM are secondary forearm stabilizers. The purpose of this study was to show importance and stability contribution of IOM and TFCC in the forearm. With sectioning TFCC and IOM the load wasn't transmitted by ulna at all but the force was transmitted just by radius directly to radiohumeral joint. Also, the proximal migration of the radius was recognized by radial head excision or by cutting TFCC and IOM. TFCC is the major soft tissue restraint preventing radial migration. Central portion of the IOM contributes 71% to the mechanical stiffness of the forearm while the TFCC contributes more than 8%, that was previously suggested. But importance of mid IOM was proved by an experiment.

THE FOREARM COMPLEX: ANATOMY, BIOMECHANICS AND CLINICAL CONSIDERATIONS [15]

DOI: [10.1197/j.jht.2006.02.002](https://doi.org/10.1197/j.jht.2006.02.002)

Forearm rotation is important for daily life, for activities such as personal hygiene or feeding. Normal forearm supination is in the range 80 – 90° and pronation is 75 – 85°. The functional ROM is 100°. In a study by Weiss and Hasting, it was shown that anular ligament allowed to sublux radial head. This fact is leading to laxity of the PRUJ. Because of the shape differences between radial and ulna articulating surfaces, the radial head translates in addition to rotation. The radial head translates posteriorly with supination and anteriorly with pronation. The central band of the IOM is the main structure responsible for longitudinal stability of forearm. Hotchikiss et al. found a 71% decrease in axial stiffness with sectioning the central band. There are studies with some conflicting results concerning the mechanics of IOM. Some of them say that the strain in IOM is the highest in the neutral position when the IOM is fully stretched. Others has stated that central band is isometric. It means that the length does not change with the pro/supination. Nakamura et al. conducted by using MRI that in the IOM there are greatest dynamic changes with forearm rotation. They made a conclusion that fibrosis of IOM after trauma may produce forearm rotation contracture. IOM has a very limited ability to heal. The PRUJ, IOM, and DRUJ are united in the sense of work that they are producing to rotate the hand. They are acting as one joint. Injury to one of these areas may be responsible for injury or mechanics change of any of other areas.

TILT OF THE RADIUS FROM FOREARM ROTATIONAL AXIS RELIABLY PREDICTS ROTATIONAL IMPROVEMENT AFTER CORRECTIVE OSTEOTOMY FOR MALUNITED FOREARM FRACTURES [16]

DOI: [10.18999/NAGJMS.74.1-2.167](https://doi.org/10.18999/NAGJMS.74.1-2.167)

The forearm rotation is realized around an axis connecting the center of the radial head and fovea of the distal ulna. This study demonstrates the difference between forearm axis of rotation and the axis of proximal radius in the treatment of malunited forearm fractures. Proximal radius tilt was defined as the angle between the rotational axis of the forearm and the axis of the proximal radius. To improve forearm pro/supination ROM, the corrective osteotomy was planned to reduce the radial tilt.

The hypothesis was that increased differences between the axis of forearm and proximal radius would be associated with increased deterioration of the pro/supination trajectory. Angular deformity of the forearm affects forearm rotation, so the treatment should be provided as a treatment of ulna and radius as a complex joint. The alignment of both bones is important for proper trajectory followed by radius during rotation. No reports have clarified how deformity of the axis of rotational movement affects forearm rotation. Bones, ligaments, and soft tissues would affect pro\supination. The bones alignment provides the primary effects on forearm rotation.

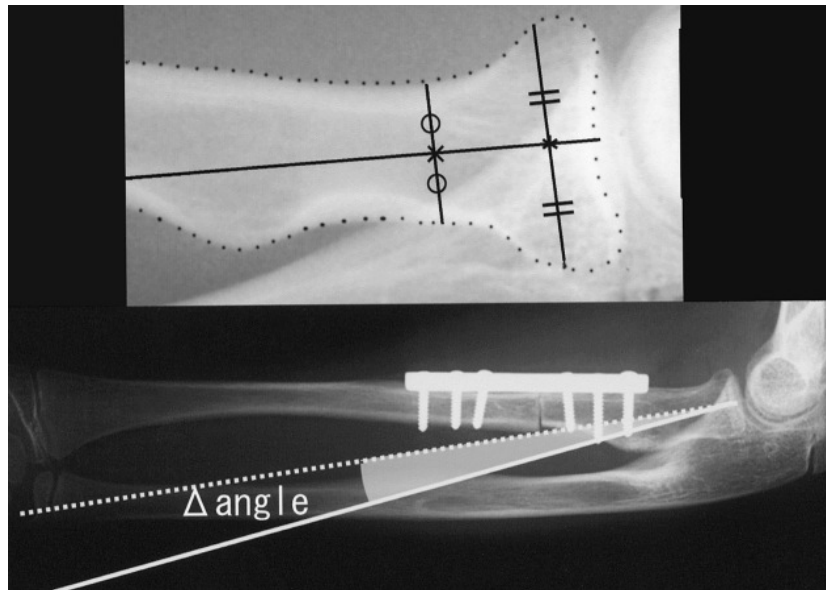


Fig. 6 – Radial tilt [16]

RECONSTRUCTION OF MALUNITED DIAPHYSEAL FRACTURES OF THE FOREARM [17]

DOI: [10.1007/s11552-014-9635-9](https://doi.org/10.1007/s11552-014-9635-9)

Radius and ulna form together a dynamic functional unit. IOM is maintaining the length of forearm and stands for longitudinal stability. The central and dorsal oblique band are responsible for PRUJ stability. DRUJ stability is represented by the distal membranous portion. The supinator, pronator quadratus, and pronator teres apply deforming forces upon fracture fragments leading to stretching of the interosseus membrane and altered rotation. The radio ulnar stability is held by elbow joint capsule and anular ligament proximally and distally by the TFCC.

Morrey et al. recognized that daily life activities require 50° of pronation and 50° of supination. For the modern activities the higher ROM is needed. Angular deformities lead to stiffness and restricted motion as the effect of stretching the IOM.

The pre-operative planning is essential. For correcting the angular deformities. Also, the simulation of pre and post operative motion simulation has been utilized. The 3D virtual operation is done stepwise. Firstly, the overlay drafting using the contralateral forearm is used. In order to determine the angle of malunion. The aim is to restore the radial anatomical arc.

3. AIM OF THE WORK

Current 3D preoperative softwares lack the precise human body kinematics. Especially, the forearm post operative ROM is not considered, that is crucial for patient's quality of life. The aim of this thesis is to propose an innovative approach to solve forearm kinematics of normal and pathological forearm. The innovative approach is based on function of PRUJ, IOM, and DRUJ ligamentous system during the pathological rotation.

- 1) We hypothesize that small malunion affects the ROM significantly by acting as closed kinematics chain.
- 2) We hypothesize that stiffness of DRUJ affects the ROM significantly.

Specific aims:

1. Define three-dimensional dynamic center of rotation of pro/supination movement.
2. Define the method for malunion model of the forearm.
3. Consider soft tissues and ligaments in the model.
4. Simulate a ROM of radius during the pathological rotation of the forearm.
5. Verify the kinematical model using clinical data.

4. METHODS

The methods are considering a description of stepwise process of building a pre and post operative forearm kinematics simulation. The only input that must be obtained are CT scans of a patient. Final output is the kinematics visualization and ROM of the patient. For all computations was used software MATLAB (R2022a, The MathWorks, Inc., Natick, Massachusetts, United States).

4.1. DATA PREPARATION

In order to realize the most precise kinematical model of forearm original geometry of bones was used. Firstly, CT pictures of bones of forearm complex (ulna, radius and distal end of humerus) were needed. For this purpose, the CT scans in DICOM file were used of normal forearm that belongs to the specific patient. The patient was 30 years old man.

The aim was to obtain the 3D models of bones from the CT scans. Image processing was used for this conversion, exactly 3D Slicer (Fedorov A., Beichel R., Kalpathy-Cramer J., Finet J., Fillion-Robin J-C., Pujol S., Bauer C., Jennings D., Fennessy F., Sonka M., Buatti J., Aylward S.R., Miller J.V., Pieper S., Kikinis R. 3D Slicer as an Image Computing Platform for the Quantitative Imaging Network. *Magnetic Resonance Imaging*. 2012 Nov;30(9):1323-41. PMID: 22770690) was used.

3D Slicer is a visualization tool widely used in clinical and research environment in medicine. It allows exploration of the imaging datasets in two, three and four dimensions. [18] The output is STL file that can be 3D printed, used in MATLAB, or edited in CAD/CAM software.

DICOM data

DICOM, it means Global Standard for Digital Medical Image Data Management. It defines the structure of data files containing the image and descriptive information about the procedure, patient, medical facility or diagnosis. The resolution is defined in px/mm. DICOM carries also information about distance of slices and their order, the position of the object in the scanner, grayscale bit depth of image and material properties. With increasing resolution and decreasing distance between slices, the stored image information becomes more detailed. [19]

Segmentation

This process is about image evaluation. ROI is segmented in order to get 3D visualization of demanded object. The artifacts such as noise round the surface of the goal object or movement during scanning are discovered. This can be removed by filtration and by usage of special algorithms for reconstruction of 2D image. [19]

Segmentation offers many algorithms to evaluated the CT scans in DICOM file. It provides also algorithms for extraction unwanted objects. There are two main algorithms for ROI 3D visualization: Grow from seeds and Thresholding (Fig. 7).

Grow from seeds

This algorithm is based on the marking the bone and background. Background stands for unwanted structures in segmentation. The marking is done by function Paint. Each entity has own color to show the difference between a bone and other structures for Grow from seeds algorithm. This algorithm is very strong and can be precise but it is time consuming and challenging for computer performance.

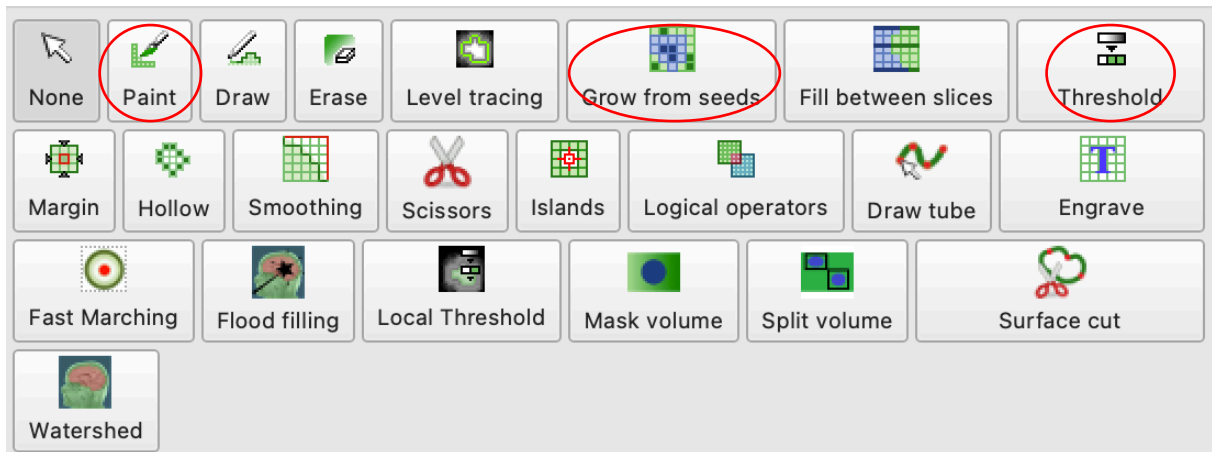


Fig. 7 – 3D Slicer, segmentation options

Thresholding

Thresholding is based on grayscale recognition, that express the absorption of radiation in the material relative to water in the so-called Hounsfield scale. The scale is described by Hounsfield Unit (HU) in the range of 4096 values from -1024 for air to +3071 for tooth enamel. HU is related to the mechanical properties of the tissue (density and modulus of elasticity). Finally, threshold effect is adjusting the image information to make the highlighting of the studied objects in the background based on gray levels. [19]

Thresholding v. Grow from seeds

The visualization of 3D Slicer output is done in the software MeshLab (P. Cignoni, M. Callieri, M. Corsini, M. Dellepiane, F. Ganovelli, G. Ranzuglia MeshLab: an Open-Source Mesh Processing Tool Sixth Eurographics Italian Chapter Conference, page 129-136, 2008).

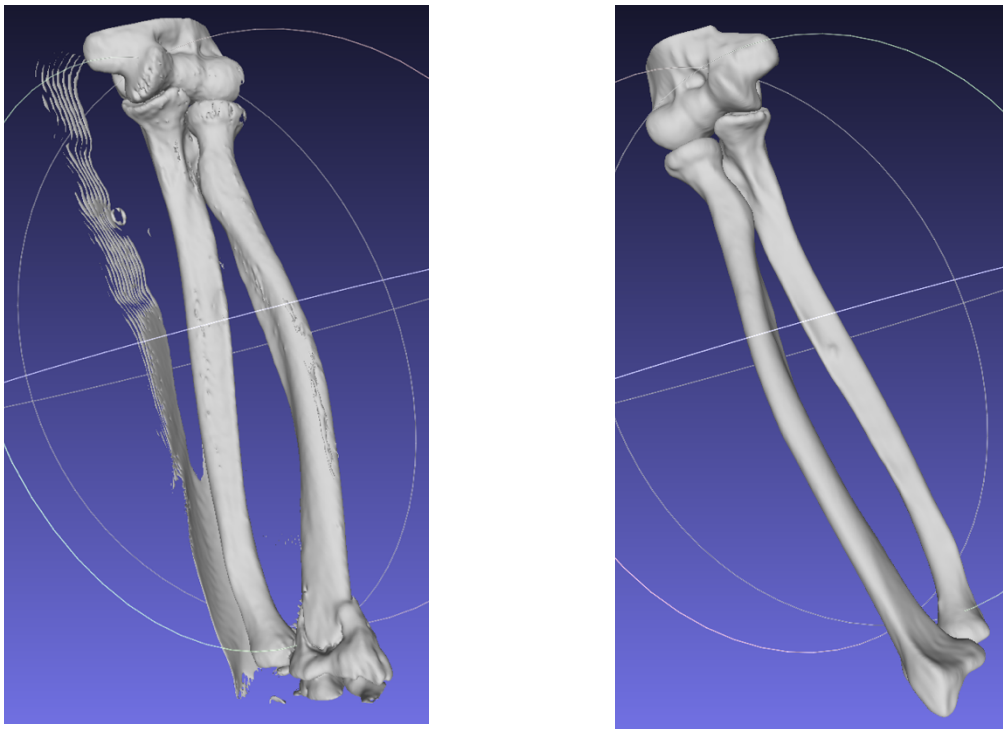


Fig. 8 – (left) Comparison of thresholding and (right) grow from seeds algorithm

Finally, algorithm Grow from seeds was used. It is possible to see that Thresholding can't deal with filtering out the hand pad or with extracting some unwanted bones such as wrist bones. The bones also are not fully closed. High porosity is observed. This is a huge issue for 3D printing (Fig. 8)

Thresholding is fast and easy method it couldn't be used in this case. It is necessary to extract the bones for kinematics modeling. That wouldn't be also possible with Thresholding.

Summary of data processing in 3D Slicer

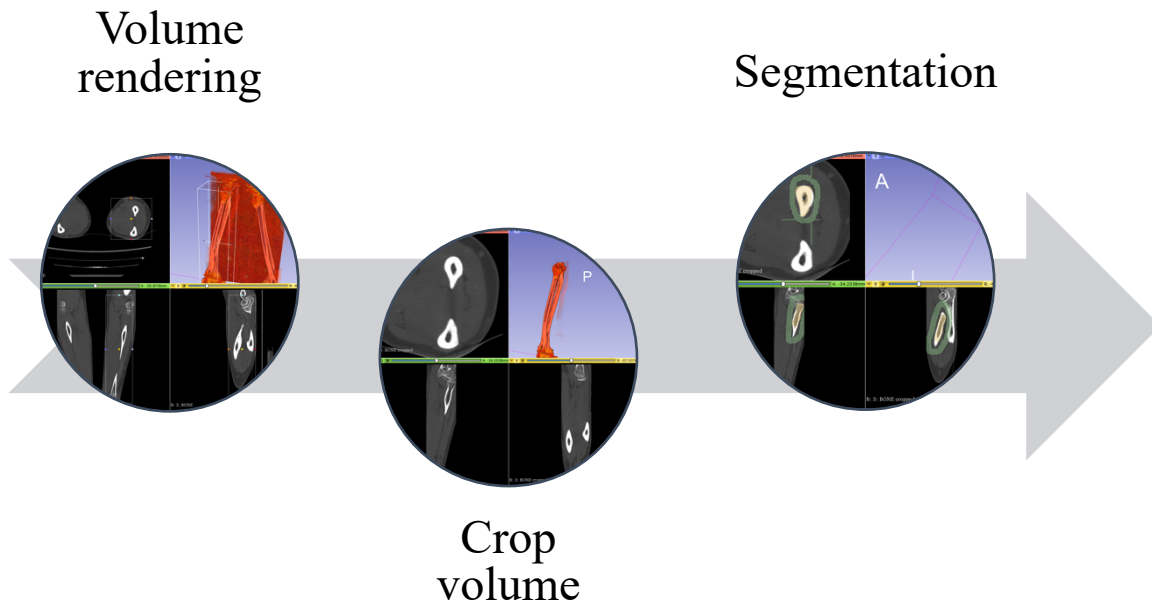


Fig. 9 – 3D Slicer procedure schema

3D Reconstruction

After finishing the whole process in 3D Slicer, the STL files of bones are created and can be exported for 3D printing or for next editing. Because of huge and precise STL mesh from 3D Slicer the mesh reduction was done for faster computations in MATLAB. The mesh of all bones was reduced in software Fusion 360 (Autodesk® Fusion 360®). Afterward the bones STL files were exported to MATLAB.

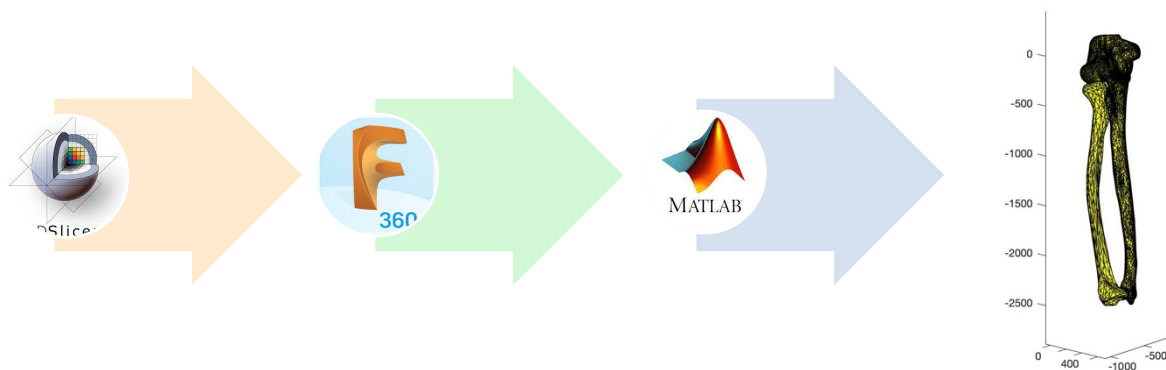


Fig. 10 – STL reconstruction procedure to MATLAB

In the Fig. 10 it is possible to see the output of the data preparation: final visualization of forearm complex. It is also recognizable that the static parts (distal end of humerus and ulna) of forearm complex have more vertices and faces. It is because their position is not time dependent and therefore is not necessary to compute many equations in many steps. This is also the purpose of mesh reduction in the second step. (Fig. 10) Faces reduction helps to faster computation of surface intersection algorithm. Initially, the STL output of radius from 3D Slicer had 40898 faces, it was reduced to 2750 faces. The STL output of ulna from 3D Slicer had 42947 faces, it was reduced to 3249 faces.

During the 3D reconstruction in the Fusion 360 the preparation of data for creation of artificial malunions was done. It was important to split the STL body and define the axis of rotation for each type of malunion.

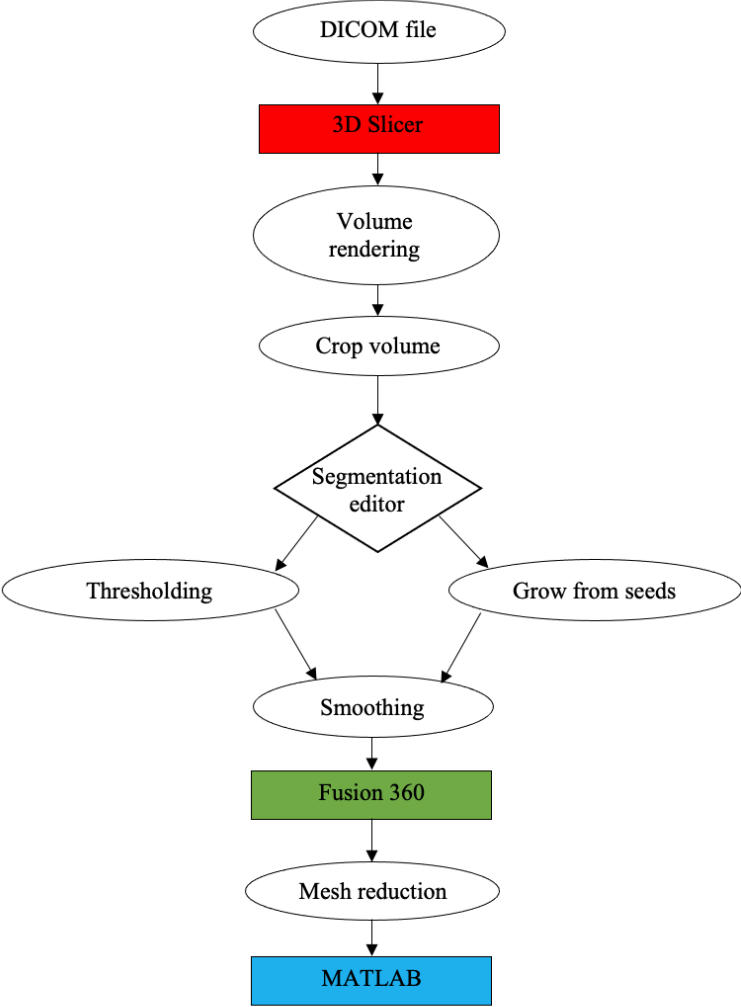


Fig. 11 – CT scans processing schema

4.2. STL SURFACE INTERSECTION

Surface intersection algorithm is crucial for contact detection. If the contact during the forearm rotation is observed between the radius and ulna, that means the restriction of pro/supination movement. Based on this algorithm the range of motion can be estimated. The STL file is composed of vertices and faces. Three vertices connects together and they are forming a triangle represented as one face.

Surface intersection algorithm was implemented externally into the MATLAB code processing the simulation of forearm kinematics. It was used as a function. The algorithm is based on Triangle – Triangle intersection test routine by Tomas Möller, 1997.

The function: Surfaceintersection.m

(<https://www.mathworks.com/matlabcentral/fileexchange/48613-surface-intersection>)

Jaroslav Tuszynski, 2014 [22]

A Fast Triangle – Triangle intersection test [23]

Let's define two triangles T_1 and T_2 . The vertices of T_1 are defined as: $\vec{V}_0^1, \vec{V}_1^1, \vec{V}_2^1$ and vertices of T_2 : $\vec{V}_0^2, \vec{V}_1^2, \vec{V}_2^2$. Two planes are denoted for both triangles as π_1 and π_2 . \vec{X} is any point in the plane.

$$\begin{aligned} \pi_2: \vec{N}_2 \cdot \vec{X} + d_2 &= 0 \\ \vec{N}_2 &= (\vec{V}_1^2 - \vec{V}_0^2) \times (\vec{V}_2^2 - \vec{V}_0^2) \\ d_2 &= -\vec{N}_2 \cdot \vec{V}_0^2 \end{aligned}$$

The distance between the vertices of T_1 and π_2 is defined as:

$$d_{V_i^1} = \vec{N}_2 \cdot \vec{V}_i^1 + d_2, i = 0,1,2$$

If the result is following:

$$d_{V_i^1} \neq 0, i = 0,1,2$$

The overlap is rejected. The same is done for T_2 and π_1 . Indeed, for a pair to pass this test there must be some line of direction $N_1 \times N_2$ that meets both.

In the case that the line is the intersection of the two planes. Both triangles intersect the line.

$$\vec{L} = \vec{O} + t\vec{D}, \vec{D} = \vec{N}_1 \times \vec{N}_2$$

\vec{D} is the direction of the line L and O is a point on it. If these intervals overlap that are intersecting on the L , the triangles overlap as well.

Code structure: [23]

1. Compute equation of triangle 2.
2. Reject as trivial if all points of triangle 1 are on same side.
3. Compute plane equation of triangle 1.
4. Reject as trivial if all points of triangle 2 are on same side.
5. Compute intersection line and project onto largest axis.
6. Compute the intervals for each triangle.
7. Intersect the intervals.

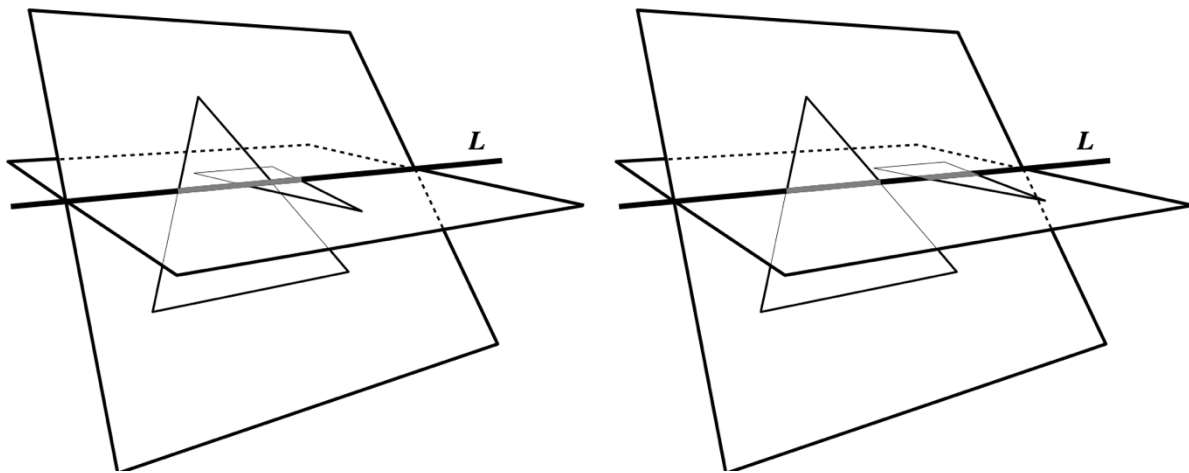


Fig. 12 – Triangle – Triangle intersection test [23]

4.3. MODELING OF NORMAL ROTATION

This chapter describes the gradual approach to real normal rotation. Attention is devoted to precise kinematical modeling of forearm pro/supination movement. Firstly, kinematics of normal forearm was described. Modeling of normal rotation consists of two iterations. In the second iteration new model of forearm kinematics was invented.

4.3.1. ONE AXIS ROTATION

The first iteration stays just for simple rotation around a defined axis of rotation, that is defined on the basis of pro/supination movement from anatomical praxis [1]. The inspiration was found in literature in sense of theoretical progression of the axis of rotation between two points. The two vectors were specified (\vec{x}_1, \vec{x}_2) that determine axis of rotation. Proximal end of axis of rotation is specified by vector \vec{x}_1 , that lies in the center of fovea radialis. The second vector \vec{x}_2 lies approximately in the center of head of ulna. The exact determination will be explained. For realization of new basis of coordinate system was necessary to state the third vector \vec{x}_3 . This vector lies on the lateral side of head of radius.

The original coordinate system is defined by three anatomical planes. Plane YZ is the frontal plane, plane XY is the transversal plane, and plane XZ is median plane.

1. Definition of 3 initial vectors in order to set up new coordinate system.

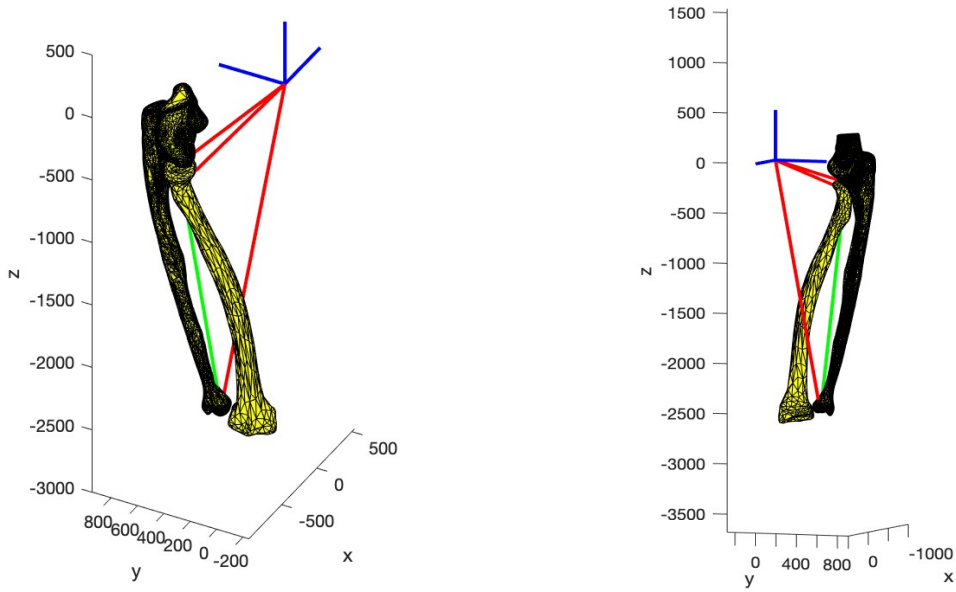


Fig. 13 – Definition of new coordinate system

$$\vec{x}_1 = \begin{bmatrix} x_{1x} \\ x_{1y} \\ x_{1z} \end{bmatrix} \quad \vec{x}_2 = \begin{bmatrix} x_{2x} \\ x_{2y} \\ x_{2z} \end{bmatrix} \quad \vec{x}_3 = \begin{bmatrix} x_{3x} \\ x_{3y} \\ x_{3z} \end{bmatrix}$$

- All the units in a coordinate system are in 10^{-4} m. This is valid for whole thesis.

2. Determination of the axis of rotation

- The rotation is realized around the vector \vec{p} (*green vector*) in 3D.
- The determination of the vector \vec{x}_2 (the vector ending in fovea of Ulna) is done by virtual experiment. The virtual experiment was done by simulating the rotation with changing the vector \vec{x}_2 until no intersection of surfaces is observed.

$$\vec{p} = \vec{x}_2 - \vec{x}_1$$

$$\vec{q} = \vec{x}_3 - \vec{x}_1$$

3. Definition of new coordinate system

- New coordinate system is set up due to better definition of rotation around one axis.
- The axis of rotation should be identical to one of the base vectors. Exactly, to vector \vec{e}_1 .
- Normalization to state new base vectors ($\vec{e}_1, \vec{e}_2, \vec{e}_3$).

$$\vec{e}_1 = \frac{\vec{p}}{\|\vec{p}\|} = [e_{1x} \quad e_{1y} \quad e_{1z}]$$

$$\vec{e}_2 = \frac{\vec{e}_1 \times \vec{q}}{\|\vec{e}_1 \times \vec{q}\|} = [e_{2x} \quad e_{2y} \quad e_{2z}]$$

$$\vec{e}_3 = \vec{e}_1 \times \vec{e}_2 = [e_{3x} \quad e_{3y} \quad e_{3z}]$$

- Matrix of direction cosines

$$\vec{\vec{R}}_0 = \begin{bmatrix} e_{1x} & e_{2x} & e_{3x} \\ e_{1y} & e_{2y} & e_{3y} \\ e_{1z} & e_{2z} & e_{3z} \end{bmatrix}$$

- Initial vector of each vertex – \vec{r}_{0n}

$$\vec{r}_{0n} = [r_{0nx} \quad r_{0ny} \quad r_{0nz}]$$

$$\vec{v}_{0n} = \vec{r}_{0n}^T - \vec{x}_1$$

$$\vec{v}_{1n} = \vec{\vec{R}}_0^T \vec{v}_{0n}$$

4. Definition of radius rotation [20]

- Definition of tensor $\vec{\vec{P}}$

$$\vec{\vec{I}} = \begin{bmatrix} 1 & 0 & 0 \\ 0 & 1 & 0 \\ 0 & 0 & 1 \end{bmatrix} \quad \vec{\vec{P}} = \begin{bmatrix} 0 & e_{1z} & -e_{1y} \\ -e_{1z} & 0 & e_{1x} \\ e_{1y} & -e_{1x} & 0 \end{bmatrix}$$

- Definition of tensor of rotation $\vec{\vec{R}}$ in 3D

$$\vec{\vec{R}} = \cos \alpha \vec{\vec{I}} + (1 - \cos \alpha) \vec{e}_1 \otimes \vec{e}_1^T - \sin \alpha \vec{\vec{P}}$$

- Rotation of each vertex

$$\vec{r}_{1n} = \vec{\vec{R}} \vec{v}_{1n}$$

Vector \vec{r}_{1n} stands for description of final position of each vertex of radius model after rotation around vector \vec{p} with incremental angle α .

4.3.2. DYNAMIC CENTRE OF ROTATION

For the second iteration the data (video) was obtained of pro/supination movement demonstrated on forearm cadaver sample (source of the video – [26]). This video was studied in a free software Tracker (Brown, W. Christian, and R. Hanson, Computer Program Tracker Video Analysis and modeling JS (beta), Version 5.9 (2020), WWW Document, (<https://tracker.physlets.org/trackerJS/>)) in order to estimate the real trajectory of radius during pro/supination. It is possible to get the trajectory points in the real case of forearm rotation with usage of Tracker. Because just the circle trajectory (simple rotation around one axis), as is

assumed in first iteration, it is not enough to converge to real movement. In fact, pro/supination is more complex rotation. In the first iteration of normal rotation, just the rotation of radius around one axis of rotation is assumed that is located in the center of ulna. This motion is possible according to bone kinematics. If just the bone kinematics is considered, a movement is important, where is no bone contact observed. In this case would be circle trajectory possible for rotational movement of radius around ulna. But if all surrounding structure such as soft tissues, muscles and ligaments are considered, the kinematics could significantly change. One of the main reasons is also the different curvature of the radius and ulna articular surfaces in DRUJ. These factors are resulting in our case in a complex rotation with dynamic center of rotation. This translating end effector of axis of rotation is causing a sliding movement of radial articulating surface on the ulna head round the neutral position. In the kinematical model it exhibits more free rotation in pronation than in supination. Unfortunately, the data analysis in Tracker from a cadaver pro/supination movement is uncompleted. Approximately last 40° of pronation is missing, so the last position of the center of rotation couldn't be precisely stated. That's why this position was estimated based on the reasonable kinematics and a fact that the TFCC is stretched and it causes a force, as a spring that is stretched, which is applied on the radius and it must translate radius back to ulna.

Generally, four positions of centers of rotation can be defined. Each position is characteristic for an interval of pronation or supination. If a man is considered with ROM 80 – 0 – 80 the intervals are 80 – 40 – 0 – 40 – 80. So, it means that the center of rotation is after a period equal to ROM/4.

Least squares method was used for circle fit to determinate the movement of center of rotation during the pro/supination. Then a general motion was obtained.

- The analytical circle equation

$$(x - x_0)^2 + (y - y_0)^2 = R^2$$

$$x^2 - 2xx_0 + x_0^2 + y^2 - 2yy_0 + y_0^2 = R^2$$

$$[-2x \quad -2y \quad 1] \cdot [x_0, \quad y_0, \quad x_0^2 + y_0^2 - R^2]^T = -(x^2 + y^2)$$

- Least squares method for circle – solving the over – determinate system [21]

$$\begin{bmatrix} -2x_1 & -2y_1 & 1 \\ \vdots & \vdots & \vdots \\ -2x_n & -2y_n & 1 \end{bmatrix} \begin{bmatrix} a \\ b \\ c \end{bmatrix} = \begin{bmatrix} -(x_1^2 + y_1^2) \\ \vdots \\ -(x_n^2 + y_n^2) \end{bmatrix}$$

$$A = \begin{bmatrix} -2x_1 & -2y_1 & 1 \\ \vdots & \vdots & \vdots \\ -2x_n & -2y_n & 1 \end{bmatrix}; B = \begin{bmatrix} -(x_1^2 + y_1^2) \\ \vdots \\ -(x_n^2 + y_n^2) \end{bmatrix}; X = \begin{bmatrix} a \\ b \\ c \end{bmatrix}$$

- This over – determined system is solved in MATLAB

$$X = A \setminus B$$

- The solution of the previous system: $a = \text{center } x - \text{coordinate}$,
 $b = \text{center } y - \text{coordinate}$, $R = \text{circle radius}$

$$a = x_0 \quad b = y_0 \quad R = \sqrt{x_0^2 + y_0^2 - c}$$

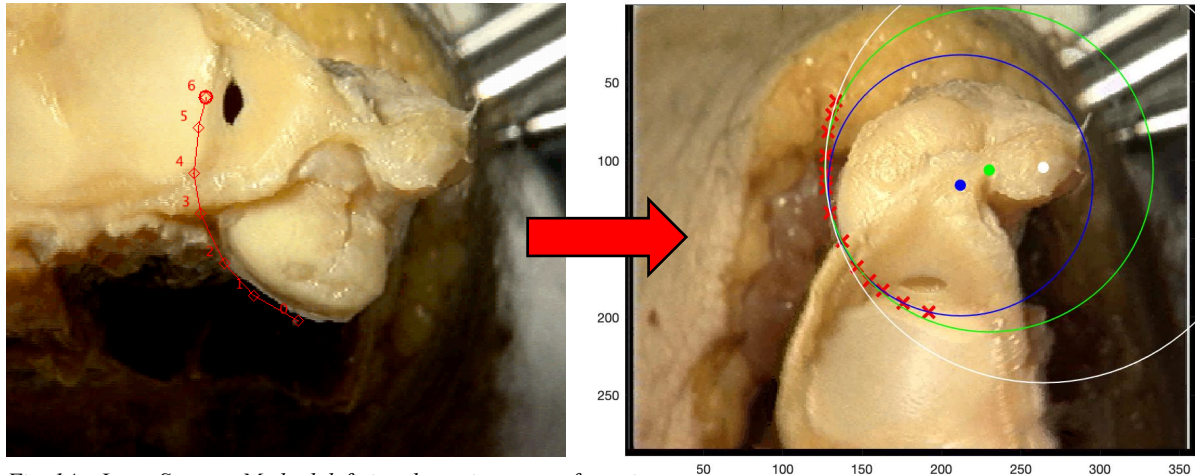


Fig. 14 – Least Squares Method defining dynamic center of rotation

The Fig. 14 shows the transition from radius trajectory reconstruction in Tracker to MATLAB least squares circle fit. The next step is implementation in to the first iteration. It means that the circle centers coordinates have to be converted from ulna cadaver picture to MATLAB 3D ulna model. This result in general motion, the center of rotation is time dependent.

Because of 2D picture from cadaver simulation the third coordinate of the center of rotation is unknown. Coordinate in y and z direction can be precisely stated. The coordinate in x direction was estimated according to the original starting center of rotation. Nevertheless, it is necessary to transfer the results from Tracker to MATLAB.

- Linear scaling to get a parameter k of vector resizing

Two dimensions are needed. The initial radius in full supination from Tracker study r_t and the same radius from MATLAB simulation r_m is needed.

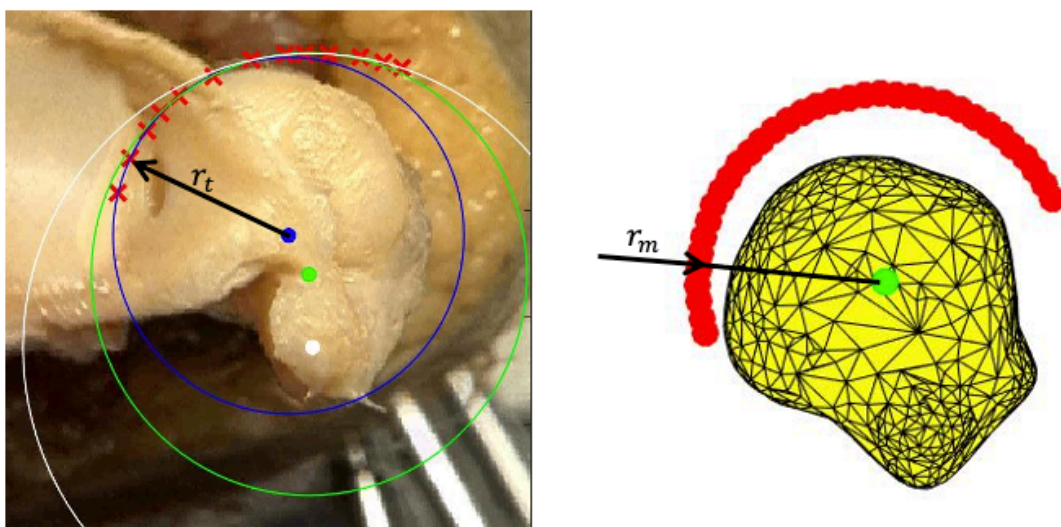


Fig. 15 – (left) Radius measurement in Tracker and (right) in MATLAB

$$r_m = k \cdot r_t$$

$$k = \frac{r_m}{r_t}$$

- Shifting vectors of center of rotation in Tracker

$$\vec{p}_{1t} = \vec{C}_2^t - \vec{C}_1^t \quad \vec{p}_{2t} = \vec{C}_3^t - \vec{C}_2^t$$

- Shifting vectors of center of rotation in MATLAB

$$\vec{p}_{1m} = k \cdot \vec{p}_{1t} \quad \vec{p}_{2m} = k \cdot \vec{p}_{2t}$$

- Equal position of centers of rotation in the MATLAB model

$$\vec{C}_2^m = \vec{C}_1^m + \vec{p}_{1m}$$

$$\vec{C}_3^m = \vec{C}_2^m + \vec{p}_{2m}$$

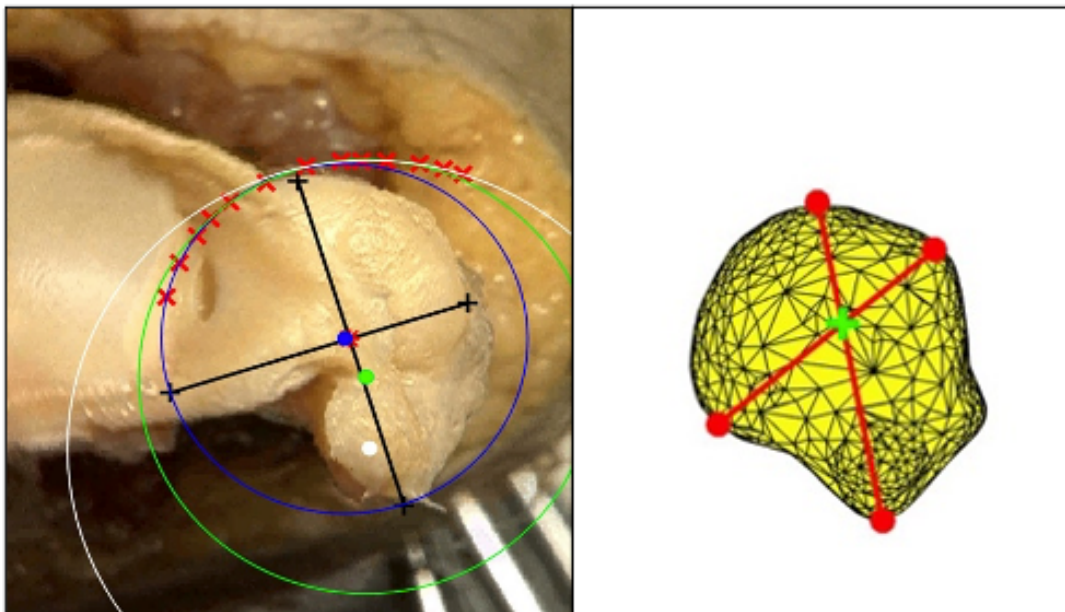


Fig. 16 – Usage of anatomical landmarks to define center of rotation

Moreover, it is possible to estimate the original starting center of rotation according to Fig. 16. The method is simple, the main four anatomical landmarks are connected by line. The intersection of line segments is defining the original starting center of rotation. This method is easy and fast. Afterwards it can be further improved in developed kinematical model. The center of rotation can be adjusted until no intersection is observed.

4.4. MALUNION MODELING

Distance of malunion from the proximal part of radius or ulna is important for malunion modeling, axis of rotation (vector) and an angle of rotation. Geometry was designed in Autodesk Fusion 360. Each forearm bone had separately own STL file. In order to rotate a distal part of a bone it was firstly necessary to split the STL body, then define (draw) the axis of rotation of malunion, that is tangential to the cross sectional cut geometry. A malunion can angulate in all body planes or in planes that are combination of them. It means the definition of 5 axis of rotation for each cross sectional cut to one bone. The lateral direction of angulation is neglected because this case is not so common. Just the angulation in medial, volar and dorsal direction and axial rotation of a distal part of bone was assumed.

Afterwards the edited model is imported into MATLAB and there could be simulated the angulation analogically to the mechanical model of rotation described in the first iteration (chapter 4.3.1) for radius rotation.

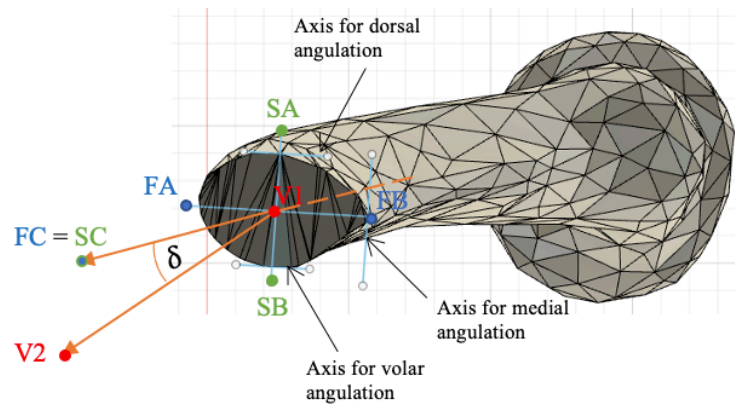


Fig. 17 – Vectors defining the kinematic of malunion

For the verification of our model, study [12] was used. Malunions are defined by two angles (δ, β). β represents angle between frontal and angulation plane. δ stands for angle between axis of proximal part of radius and angulated distal part of radius in the angulation plane. Malunion modeling procedure is based on possible angulation in two planes – sagittal (blue – Fig. 18) and frontal (red – Fig. 18) plane. The angulations from the publication [12] are implemented to our model.

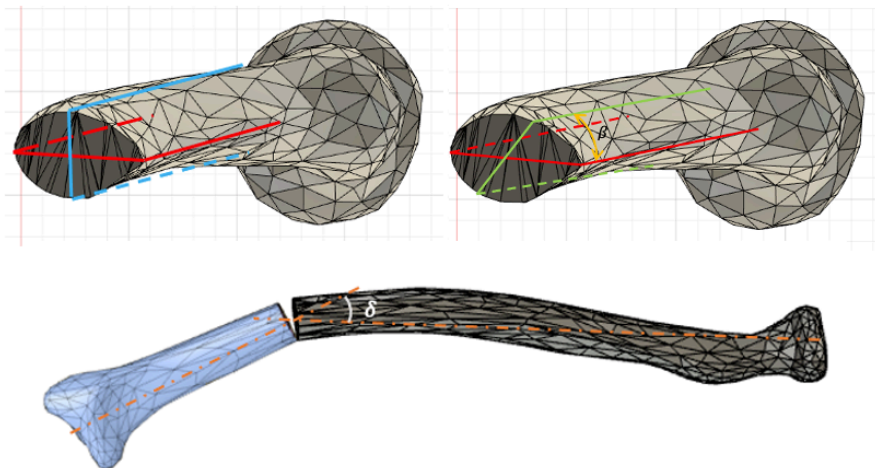


Fig. 18 – Definition of angulation plane by angle β and angle δ responsible for axial angulation

Firstly, the vector \vec{V} is defined. Vector \vec{V} represents the angulation, it is the axis of distal angulated part of radius or ulna. This vector lies in the angulated plane and it is rotated about angle δ to the axis of proximal part of the bone. Then the frontal and sagittal plane is defined. Especially, the normal vector to these planes was used – cross product. From the definition of dot product, the angle between vector \vec{V} and the frontal and the sagittal plane could be derived. These angles represent medial (ϵ) angulation and dorsal/volar (φ) angulation.

- Angulation of the frontal plane by the angle β , the rotation is around a vector \vec{J} .

$$\vec{J} = \vec{FC} - \vec{V1}$$

$$\vec{j} = \frac{\vec{J}}{\|\vec{J}\|} = [j_x \quad j_y \quad j_z] \quad \vec{P} = \begin{bmatrix} 0 & j_z & -j_y \\ -j_z & 0 & j_x \\ j_y & -j_x & 0 \end{bmatrix}$$

$$\vec{R} = \cos \beta \cdot \vec{I} + (1 - \cos \beta) \cdot \vec{j} \otimes \vec{j}^T - \sin \beta \cdot \vec{P}$$

$$\vec{F} = \vec{R} \cdot \vec{FB} - \vec{R} \cdot \vec{FA}$$

- Angulation of the radial axis \vec{J} by the angle δ , the rotation is around a vector \vec{F} .

$$\vec{f} = \frac{\vec{F}}{\|\vec{F}\|} = [f_x \quad f_y \quad f_z]^T \quad \vec{P} = \begin{bmatrix} 0 & f_z & -f_y \\ -f_z & 0 & f_x \\ f_y & -f_x & 0 \end{bmatrix}$$

$$\vec{R} = \cos \delta \cdot \vec{I} + (1 - \cos \delta) \cdot \vec{f} \otimes \vec{f}^T - \sin \delta \cdot \vec{P}$$

$$\vec{V} = \vec{R} \cdot \vec{j}^T$$

$$\vec{FAB} = \vec{FB} - \vec{FA}$$

$$\vec{FAC} = \vec{FC} - \vec{FA}$$

$$\vec{nFABC} = \vec{FAB} \times \vec{FAC}$$

$$\varphi = 90^\circ - \cos^{-1} \left(\left| \frac{\vec{V} \cdot \vec{nFABC}}{\|\vec{V}\| \|\vec{nFABC}\|} \right| \right) \frac{180^\circ}{\pi}$$

$$\vec{SAB} = \vec{SB} - \vec{SC}$$

$$\vec{SAC} = \vec{SC} - \vec{SA}$$

$$\vec{nSABC} = \vec{SAB} \times \vec{SAC}$$

$$\epsilon = 90^\circ - \cos^{-1} \left(\left| \frac{\vec{V} \cdot \vec{nSABC}}{\|\vec{V}\| \|\vec{nSABC}\|} \right| \right) \frac{180^\circ}{\pi}$$

Data		Radius			Ulna			Mobility		
Patient	Loc [%]	Angulations angles			Angulations angles			Pronation	Supination	ROM
Number	-	δ [°]	β [°]	π [°]	δ [°]	β [°]	π [°]	[°]	[°]	[°]
1	47	15	56	45	9	41	0	15	75	90
3	56	20	0	0	23	40	30	10	75	85
4	32	16	45	ND	7	0	ND	5	90	95
5	71	16	0	0	10	0	10	40	60	100
6	45	18	40	45	7	0	7	20	70	90
7	40	12	0	ND	0	0	ND	45	10	55
8	40	16	0	0	11	31	-25	70	0	70
9	55	30	45	ND	10	0	ND	90	10	100
11	56	13	18	ND	9	0	ND	70	100	170
12	66	7	0	ND	0	0	ND	70	95	165
13	77	18	40	20	0	0	0	75	70	145
14	68	13	32	ND	0	0	ND	65	100	165
15	70	20	0	ND	0	0	ND	65	80	145
17	65	20	0	ND	0	0	ND	80	90	170

Tab. 1 – Patients – Malunion definition and individual ROM [12]

Tab. 1 represents a study where the angulations of forearm bones were measured with corresponding ROM. The reconstruction of these results was done by usage of our virtual model. It served also as a verification for our model. Three patients were not considered for model verification. Patient 2, 10, 16. Patient 2 and 10 weren't able to start the pronation or supination from neutral position. Patient 16 underwent a double osteotomy, so it means more complex deformity that would be very hard to simulate.

Process of complex malunion modeling:

The rotational tensors \vec{R}_i , $i = 1,2,3$ has similar structure to the previously defined rotational tensors \vec{R} . The computation follows firstly the definition of rotation axis vector, then normalization of this vector, then construction of matrix \vec{P} and finally input of rotational angle to rotational tensor equation.

1. Axial rotation of distal radius/ulna segment around vector $\vec{v} = \vec{V}$

$$\vec{v} = \vec{V2} - \vec{V1} = \vec{R} \cdot \vec{j}^r$$

$$\vec{r}_{1dn} = \vec{R}_1 (\vec{r}_{0dn} - \vec{V1}) + \vec{V1}$$

2. Medial rotation of distal radius/ulna segment around vector \vec{m}

$$\vec{m} = \vec{M2} - \vec{M1}$$

$$\vec{r}_{2dn} = \vec{R}_2 (\vec{r}_{1dn} - \vec{M1}) + \vec{M1}$$

3. Volar/Dorsal rotation of distal radius/ulna segment around vector \vec{d}

- Firstly, we have to do medial rotation of the vectors that determinate axis of rotation for volar or dorsal angulation.

$$\begin{aligned} \overrightarrow{D12} &= \overrightarrow{R_2} (\overrightarrow{D11} - M1) + \overrightarrow{M1}; \overrightarrow{D22} = \overrightarrow{R_2} (\overrightarrow{D21} - M1) + \overrightarrow{M1} \\ \vec{d} &= \overrightarrow{D22} - \overrightarrow{D12} \\ \overrightarrow{r_{3dn}} &= \overrightarrow{R_3} (\overrightarrow{r_{2dn}} - \overrightarrow{D12}) + \overrightarrow{D12} \end{aligned}$$

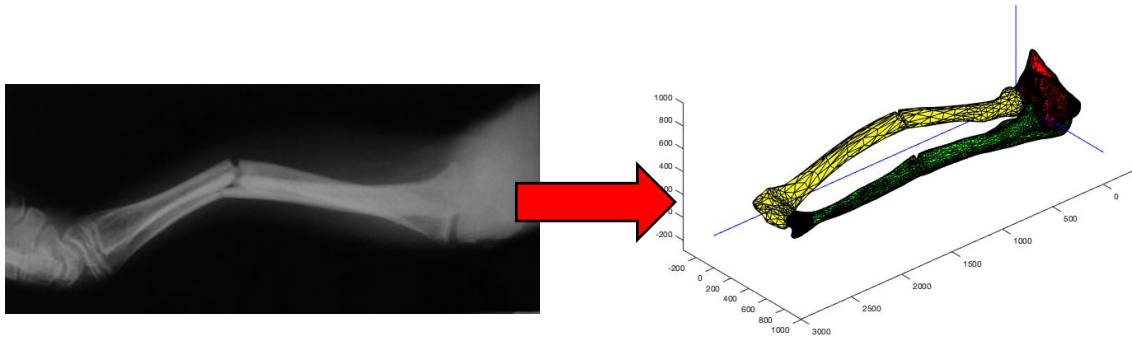


Fig. 19 – Malunion reconstruction – CT scans [25] to MATLAB angulated forearm model.

4.5. MODELING OF PATHOLOGICAL ROTATION

Precise simulation of the normal rotation and malunions was defined. By combination of these two methods together it is possible to make a model of a pathological rotation. In order to get much closer as it is possible to the real behavior of malunited forearm during pro/supination movement it is necessary to do iterations that are realized by supporting structures involved in the forearm complex. All these iterations make from forearm complex a single joint with more than one degree of freedom.

4.5.1. ROTATION CENTRE TRANSLATION BY ANGULATION

In the first iteration a factor that is caused by own kinematics of angulated bones is considered. It is the translation of the axis of rotation. This translation is constant during whole radius rotation. The distal end of the axis of rotation is translated by vector same as the vector of radius angulation of distal end of radius.

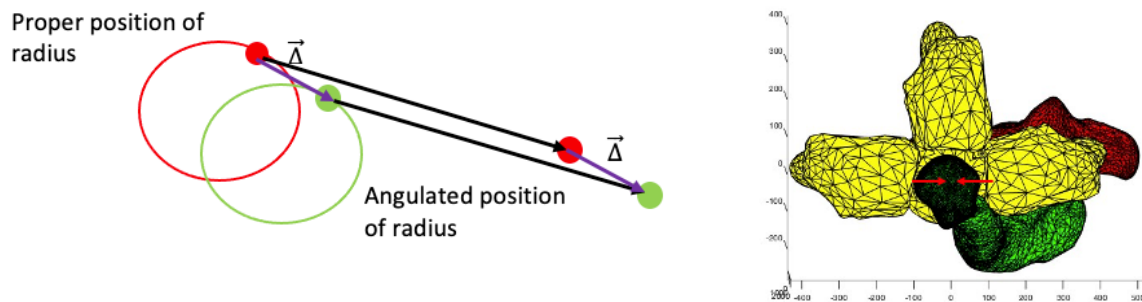


Fig. 20 – Vector translation of center of rotation by the angulation of radius

$\overrightarrow{r_{0an}}$ stands for the initial vector of angulated radius. This vector is an image of $\overrightarrow{r_{0n}}$. The difference of these two vectors is the translation vector of the distal end of axis of rotation.

$$\vec{\Delta} = \overrightarrow{r_{0an}} - \overrightarrow{r_{0n}}$$

$$\overrightarrow{x_{2a}} = \vec{\Delta} + \overrightarrow{x_2}$$

$$\overrightarrow{\Delta_s} = -\overrightarrow{\Delta_p} = |\vec{\Delta}|$$

The difference between the translation during pronation and supination is present. A hypothesis is sated that the translation vector has always a direction of the positive normal to the surface of a radius (Fig 20 – right and Fig 22.).

In the case of malunion where are involved both bones radius and ulna, end effector of axis of rotation firstly follows the ulna angulation and afterwards it is translated according to radius angulation (Fig. 21). The final configuration of axis of rotation is then represented by $\overrightarrow{x_{2b}}$.

$$\overrightarrow{x_{2a}} = \vec{\Delta}_a + \overrightarrow{x_2}$$

$$\overrightarrow{x_{2b}} = \vec{\Delta}_b + \overrightarrow{x_{2a}}$$

$$\overrightarrow{x_{2b}} = \overrightarrow{x_2} + \vec{\Delta}$$

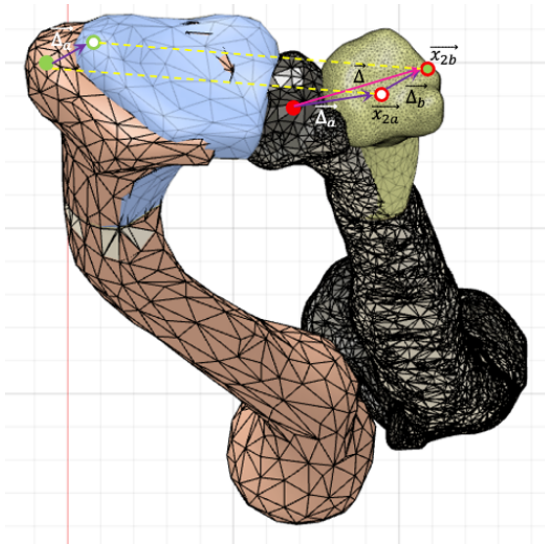


Fig. 21 – Composition of the translation vector due to radius and ulna malunion

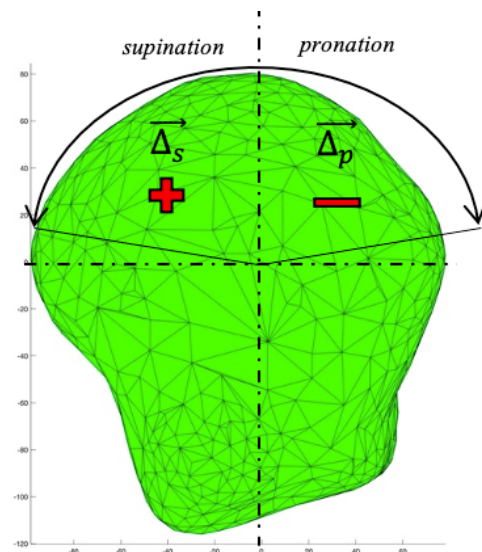


Fig. 22 – The direction of the vector $\vec{\Delta}$

4.5.2. ROTATION IN RADIOHUMERAL JUNCTION

Next factor that is influencing the pathological kinematics of forearm is ventro – dorsal and mediolateral rotation in radio – humeral junction. This rotation is limited by surrounding tissue, muscles and ligamentum anulare.

The estimation of the angle of rotation in radio – humeral junction was done by assuming simple geometrical rules (Fig. 23). The angles α_r, β_r are known, the angles of a malunion and the angles θ, ξ are to be found. The rotation in PRUJ must compensate displacement of the distal radius.

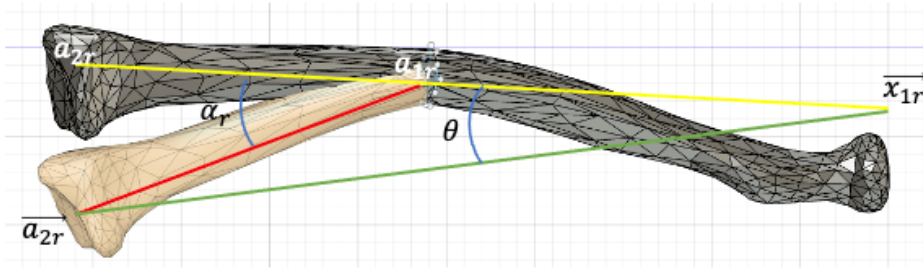


Fig. 23 – Geometry for an estimate of radiohumeral rotation

Conditions results geometrical equality:

$$\theta \|\vec{x}_{1r} - \vec{a}_{2r}\| = \alpha_r \|\vec{a}_{1r} - \vec{a}_{2r}\|$$

$$\xi \|\vec{x}_{1r} - \vec{a}_{2r}\| = \beta_r \|\vec{a}_{1r} - \vec{a}_{2r}\|$$

From this can be derived:

$$\theta = \alpha_r \frac{\|\vec{a}_{1r} - \vec{a}_{2r}\|}{\|\vec{x}_{1r} - \vec{a}_{2r}\|}$$

θ stands for angle representing ventro – dorsal rotation in neutral position. The Fig. 24 on the left is showing this exaggerated rotation.

$$\xi = \beta_r \frac{\|\vec{a}_{1r} - \vec{a}_{2r}\|}{\|\vec{x}_{1r} - \vec{a}_{2r}\|}$$

ξ stands for angle representing medio – lateral rotation in neutral position. β_r is in this case angulation angle for volar or dorsal malunion. The Fig. 24 on the right is showing this exaggerated rotation.

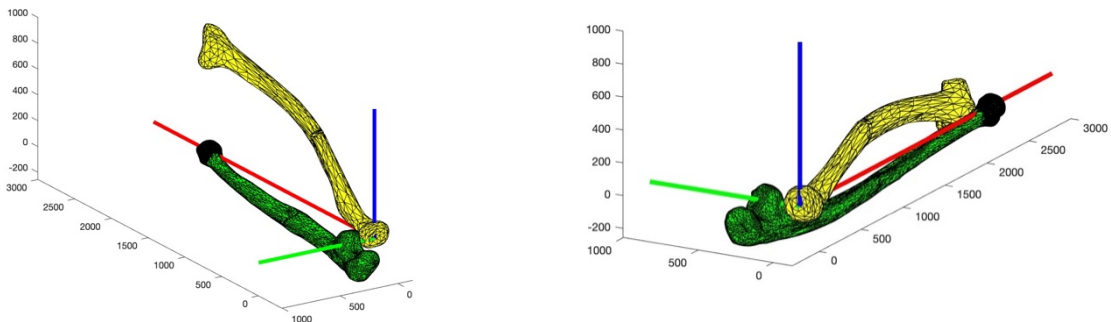


Fig. 24 – (left) Exaggerated ventro – dorsal rotation and (right) exaggerated medio – lateral

The rotation in radiohumeral junction is possible around two mutually perpendicular axes. Generally speaking, this iteration cause increase of stress in the IOM [12]. This increased stress leads to higher contact pressure in the DRUJ. It could be schematically showed in the Fig. 25. It demonstrates the kinematics of IOM after the propagation of deformity and subsequent reaction in the radiohumeral junction. The IOM could be assumed as a nonlinear spring.

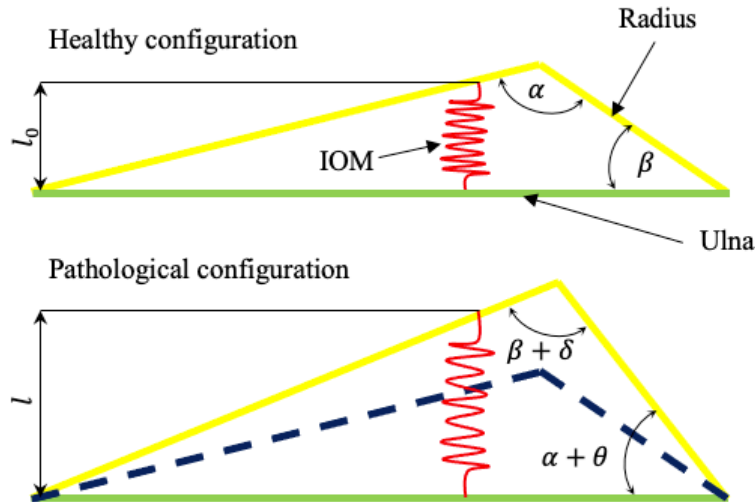


Fig. 25 – Simplification of the IOM mechanics during the angulation of radius

In the normal configuration could be imagen anatomical curvatures replaced by natural angles α, β . These angles change in the pathological configuration ant it elongates the IOM ligaments, the spring. So, the final force of a spring, that is creating the contact pressure in DRUJ is derived as:

$$F = k_{IOM} \cdot (l - l_0)$$

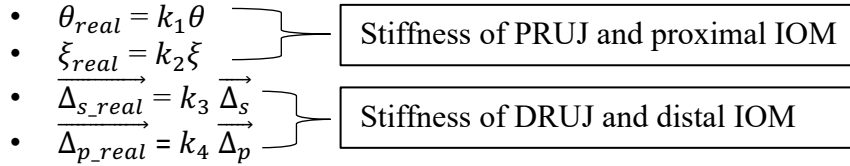
The k_{IOM} is the stiffness of the IOM that is unknow. But from the next iteration, it could be estimated.

4.5.3. MODEL SET UP BY STIFFNESS PARAMETRES

The translation is in reality much smaller because of ligamentous complex binding ulna and radius together. In the third iteration the forearm pathological kinematical model considers the effectivity and the stiffness of ligaments, muscles and surrounding tissue. It is very hard to exactly determinate the physical parameters of all influencing factors. That's why four parameters that take in account all these above-mentioned factors were defined. These four parameters are related to the translation of axis of rotation and rotation in radiohumeral junction. Their purpose is to restrain the additional movements caused by malunion. Without these coefficients the theoretical value of parameter $\vec{\Delta}$ would be unreal because of presence of TFCC. In fact, the translation of axis of rotation is dependent on stiffness of TFCC, distal IOM and other ligaments in the distal part of forearm. So, there are two coefficients representing the stiffness of DRUJ and IOM.

The rotation in radiouhumeral joint has own theoretical values according to original malunion, nevertheless the precise value of rotational angles in radiohumeral joint is unknown by each single patient. The main factors affecting pathological movement in radiohumeral joint are the stiffness of ligamentum anulare and stiffness of proximal IOM. So, there are another two coefficients representing the stiffness of PRUJ and IOM.

Model setup:



In the other words, the parameters are a ratio between real and theoretical value. The theoretical value doesn't consider the mechanics of ligaments and soft tissues.

Population:

$$\vec{p} = [k_1 \quad k_2 \quad k_3 \quad k_4]$$

Lower and upper bound:

$$p_i \in \langle 0,1 \rangle$$

- 0 => absolutely stiff (k_1, k_2)
- 1 => absolutely compliant (k_1, k_2)
- 0 => absolutely compliant (k_3, k_4)
- 1 => absolutely stiff (k_3, k_4)

Changing the population of coefficients, the pathological rotation of forearm can be precisely set up for a single patient with original malunion.

Optimization was used for setting up the coefficients. From the optimization methods the most convenient are global methods such as genetic algorithms or simulated annealing. Minimalization problem of cost function is being solved.

Simulated annealing (SA):

$$CF: \min \left\{ (ROM_{pro} - ROM_{p_real})^2 + (ROM_{sup} - ROM_{s_real})^2 \right\}$$

- LB = 0; UB = 1
- Cooling parameter: $T = T_0 \cdot 0,95^n$
- Initial temperature: $T_0 = 100^\circ$
- Metropolis criterion: $e^{\frac{\Delta E}{kT}}, \Delta E = new\ solution - old\ solution$ [24]

In order to set up the model using SA real measured ROM data are needed of a particular patient. Cost function is being minimalized based on the difference of real ROM in pronation/supination and ROM that is computed by our simulation. The SA must run the code in each iteration. The current ROM is computed as the result of a rotation without contact.

This optimization process is time demanding that's why it is necessary to speed it up by some modifications of the code. Firstly, the STL files of ulna and radius were reduced just to contact surfaces of distal ends of both bones (Fig. 26). Secondly, the code terminates when contact of the faces is detected. Also, the step of the rotational angle is adjusted. The recommended value is between 5° and 10°.

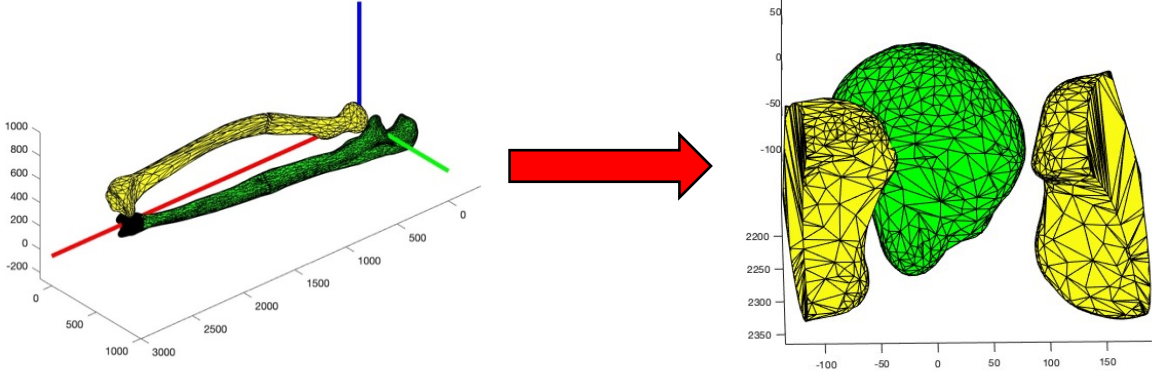


Fig. 26 – Consideration of articulating surface for SA algorithm

SA – realization:

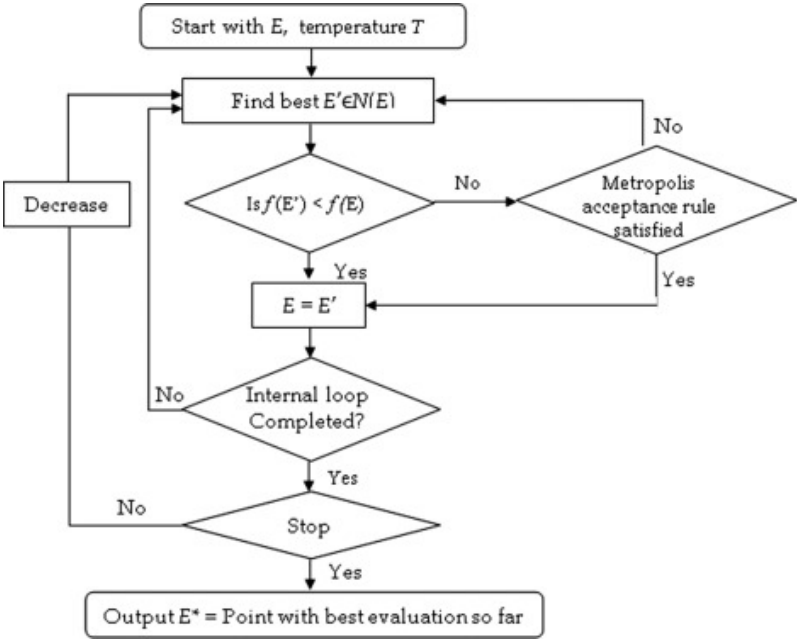


Fig. 27 – SA scheme [24]

For the first iteration initial guess is needed and then this cycle is repeated until we the cost function value is sufficiently low, in the best case it is equal to zero.

4.5.4. LONGITUDIANAL RADIUS TRANSLATION

This final iteration representing longitudinal translation of radius during the pathological rotation. The radius can displace along its longitudinal axis that is defined by \vec{p}_r , where \vec{x}_{2r} is the vector marking the end effector of radius.

$$\vec{x}_{2r} = [x_{2rx} \quad x_{2ry} \quad x_{2rz}]$$

- \vec{x}_1 vector marking center of fovea radialis.

$$\vec{p}_r = \vec{x}_{2r} - \vec{x}_1^T$$

- Formation of a new basis leading to new coordinates system for radius.

$$\vec{e}_1 = \frac{\vec{p}_r}{\|\vec{p}_r\|} = [e_{1x} \quad e_{1y} \quad e_{1z}]$$

$$\vec{e}_2 = \frac{\vec{e}_1 \times \vec{q}}{\|\vec{e}_1 \times \vec{q}\|} = [e_{2x} \quad e_{2y} \quad e_{2z}]$$

$$\vec{e}_3 = \vec{e}_1 \times \vec{e}_2 = [e_{3x} \quad e_{3y} \quad e_{3z}]$$

$$\vec{R}_0 = \begin{bmatrix} e_{1x} & e_{2x} & e_{3x} \\ e_{1y} & e_{2y} & e_{3y} \\ e_{1z} & e_{2z} & e_{3z} \end{bmatrix}$$

- Transfer to coordinates system of radius and the longitudinal translation by vector \vec{t} .

$$\vec{v}_{0n} = \vec{r}_{0n}^T - \vec{x}_1$$

$$\vec{v}_{1n} = \left(\vec{R}_0^T \vec{v}_{0n} \right) + \vec{t}$$

- Displaying the new position of the radius in the original coordinate system.

$$\vec{v}_{2n} = \left\{ \left[\text{inv} \left(\vec{R}_0^T \right) \vec{v}_{1n} \right] + \vec{x}_1 \right\}^T$$

Generally, it is known that there are existing some translations like they are described above but due to complexity of our model and a lack of knowledge about this phenomenon, was considered negligible in further analysis.

4.6. CLINICAL PROCESS OF 3D PREOPERATIVE KINEMATICS PLANNING

Surgical case:

CT scans of a malunited forearm are given. The patient is 13 years old boy. Firstly, the reconstruction of the CT scans to 3D models is done.

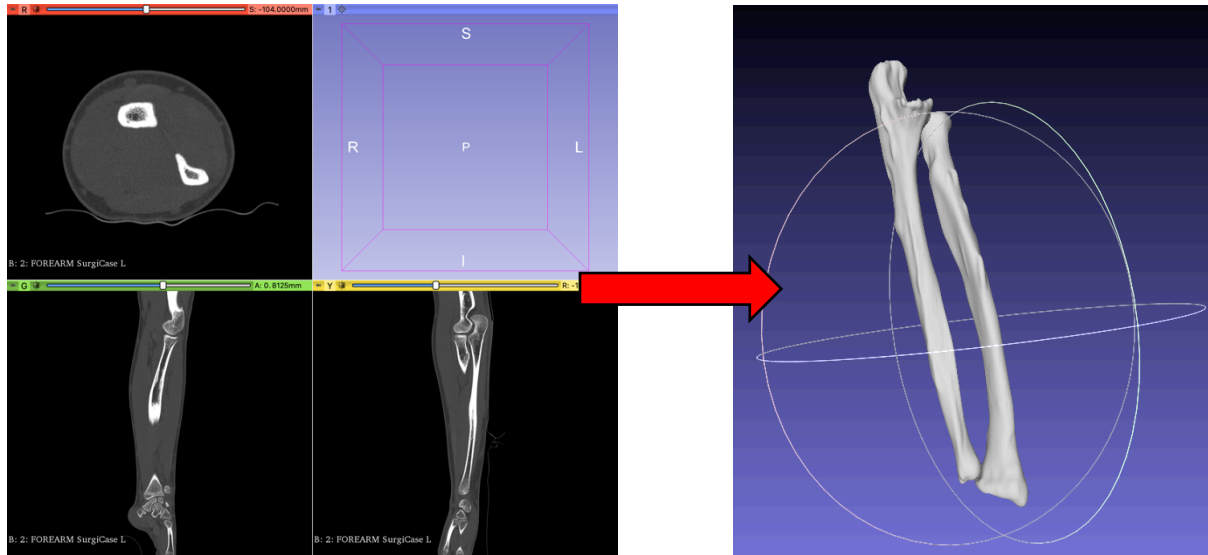


Fig. 28 – CT scans reconstruction in the 3D Slicer to 3D model

The 3D reconstruction is done as is described in the chapter 4.1., the common way how to do a reconstruction is to use 3D Slicer.

The results of this step are separate STL files of radius and ulna. The same procedure for both forearms is done.

Mirroring:

Consequently, it is necessary to make sure whether right forearm is not malunited. Then the left and right forearm bones can be compared in order to see the angulation. Mirroring is done by the alignment of the bones of the same type to a unique axis. The Alignment is done by rotational tensors explained in the chapter 4.3.1.

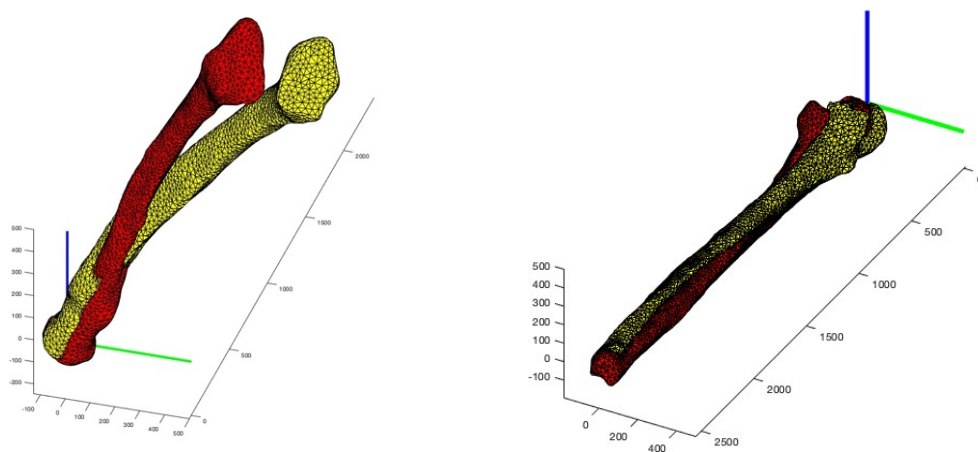


Fig. 29 – (left) Mirroring of radius and (right) ulna in MATLAB

Kinematics simulation:

1) Step and maximal ROM adjustment

By setting the step, the increment is defined, which defines the smoothness of the movement. Step 5° is chosen. The finer the step is, the more accurate the ROM estimation simulation. Next, maximal ROM has to be set. Maximal ROM varies for supination between $80^\circ - 85^\circ$ and for pronation it is $75^\circ - 80^\circ$ [15].

2) Input vectors

$$\vec{x}_1 = \begin{bmatrix} x_{1x} \\ x_{1y} \\ x_{1z} \end{bmatrix} \quad \vec{C}_1^m = \vec{x}_2 = \begin{bmatrix} x_{2x} \\ x_{2y} \\ x_{2z} \end{bmatrix} \quad \vec{x}_3 = \begin{bmatrix} x_{3x} \\ x_{3y} \\ x_{3z} \end{bmatrix} \quad \vec{C}_2^m = \begin{bmatrix} c_{2x} \\ c_{2y} \\ c_{2z} \end{bmatrix} \quad \vec{C}_3^m = \begin{bmatrix} c_{3x} \\ c_{3y} \\ c_{3z} \end{bmatrix}$$

These vectors $\vec{x}_n, n = 1,2,3$ represent new base vectors. Vectors $\vec{C}_n^m, n = 1,2,3$ represent the centers of rotation in the original state or after ulna malunion if it is present.

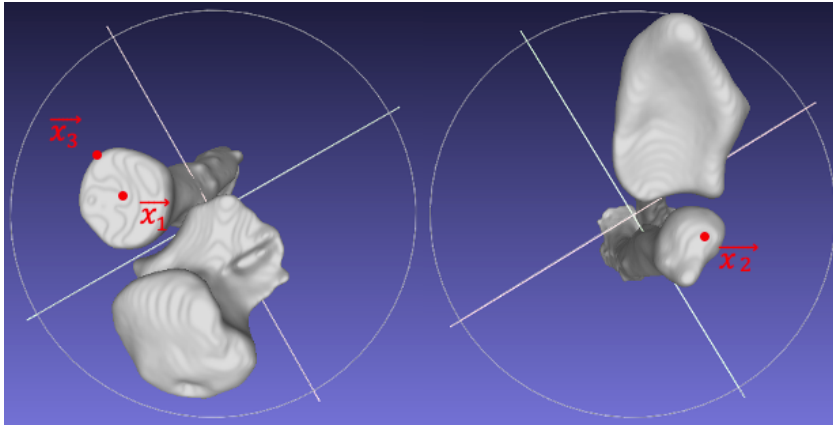


Fig. 31 – Initial vectors definition

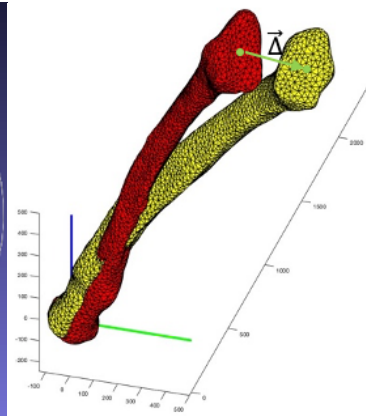


Fig. 30 – Definition of translation vector $\vec{\Delta}$

Next vector that has to be stated: $\vec{\Delta}$, this vector follows the angulation of radius and it will translate the centers of rotation.

3) Parameters set up k_3, k_4

To describe the effect of soft tissues and presence of TFCC and IOM, parameters k_3, k_4 can be involved into our model. For the initial estimation it is possible to set up them on the middle value -0.5 . Parameters k_1, k_2 don't have to be used because the initial malunited configuration was obtained in the neutral position.

4) STL input data

```
importstlR = stlread('Radius_Left.stl');
importstlU = stlread('Ulna_Left.stl');
```

```
VR = importstlR.vertices;
FR = importstlR.faces;
VU = importstlU.vertices;
FU = importstlU.faces;
```


Import the data and assign the single matricides for faces and vertices. Vertices represent each vector of the STL object and they are used for kinematic description.

5) Coordinates system origin plot

$$\vec{O}_1 = \begin{bmatrix} 0 \\ 0 \\ 0 \end{bmatrix} \quad \vec{e}_1 = \begin{bmatrix} 1 \\ 0 \\ 0 \end{bmatrix} \quad \vec{e}_2 = \begin{bmatrix} 0 \\ 1 \\ 0 \end{bmatrix} \quad \vec{e}_3 = \begin{bmatrix} 0 \\ 0 \\ 1 \end{bmatrix}$$

6) New basis setting

The MATLAB procedure to rotate whole system to new basis with origin in basic coordinate system. In detailed it is described in chapter 4.3.1.

$$\begin{aligned} a &= x2-x1; \\ b &= x3-x1; \\ e1 &= a/norm(a); \\ e2 &= cross(e1,b)/norm(cross(e1,b)); \\ e3 &= cross(e1,e2); \\ R1 &= [e1(1) e2(1) e3(1); e1(2) e2(2) e3(2); e1(3) e2(3) e3(3)]; \end{aligned}$$

$$\begin{aligned} VU0 &= VU'-x1'; \\ VU1 &= R1'*VU0; \end{aligned}$$

$$\begin{aligned} VR0 &= VR'-x1'; \\ VR1 &= R1'*VR0; \end{aligned}$$

7) Rotation

$$\begin{aligned} C1 &= C1+delta'*k3; \\ C2 &= C2+delta*k3; \\ C3 &= C3-delta*k4; \\ C4 &= C4-delta*k4; \end{aligned}$$

- Supination

```
for alfa = 1: number of steps sup+1
    if alfa ≤ number of steps sup/2+1
        end position = Rotation (step*alfa-alfa, O1, C1, VR)
    else
        end position = Rotation (step*alfa, O1, C2, VR)
    end
    if contact
        ROM = 0
        break
    else
        ROM = 1
    end
end
```

- Pronation

```

for alfa = 1: number of steps pro
  if alfa ≤ number of steps pro/2
    end position = Rotation (-step*alfa, O1, C2, VR)
  else
    end position = Rotation (step, O1, C4, VR)
  end
  if contact
    ROM = 0
    break
  else
    ROM = 1
  end
end
end

```

This is the pseudo code for the kinematics algorithm without the visualization. The function of rotation is described by mathematical expressions in the chapter 4.3.1. First argument stands for the angle of rotation, second and third argument are stating the vector of rotation and last argument is the matrix of end effectors to be rotate.

8) Output definition

The output is separately ROM in the pronation and in the supination.

```

ROM sup = [double]
ROM pro = [double]

```

```

fprintf('ROM (pronation[°]/supination[°]): %d - 0 - %d\n',ROM_pro,ROM_sup)

```

Usage of static preoperative 3D softwares:

A surgeon does the virtual operation in a 3D preoperative software where the surgeon is able to simulate post operative state. This post operative state can be once again exported as STL file and it can undergo our kinematics software to see the post operative ROM.

Code diagram:

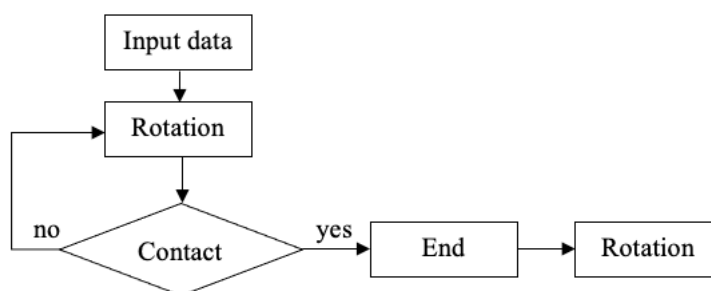


Fig. 32 – Rotation algorithm schema

5. RESULTS

The results are covering the step – by – step visualization of forearm kinematics during normal and pathological pro/supination movement. The importance of all iterations during the simulation is shown. All factors considered in our model significantly influencing the resulting ROM. The resulting information that is possible to achieve from our model is to preoperatively predict the ROM if some deformities are during the operation not eliminated or some imperfections occur.

5.1. NORMAL ROTATION

In the Fig. 33 there are shown three different situations. The picture in the left exhibits the trajectory of simple rotation around one axis. The picture in the middle stands for the visualization of the proper trajectory of radius, trajectory of general motion. The trajectory is divided by colors in to the four sections. The sections represent an interval with constant radius during the rotation. In the picture in the right is the comparison between one axis rotation (red) and general motion (blue) of radius.

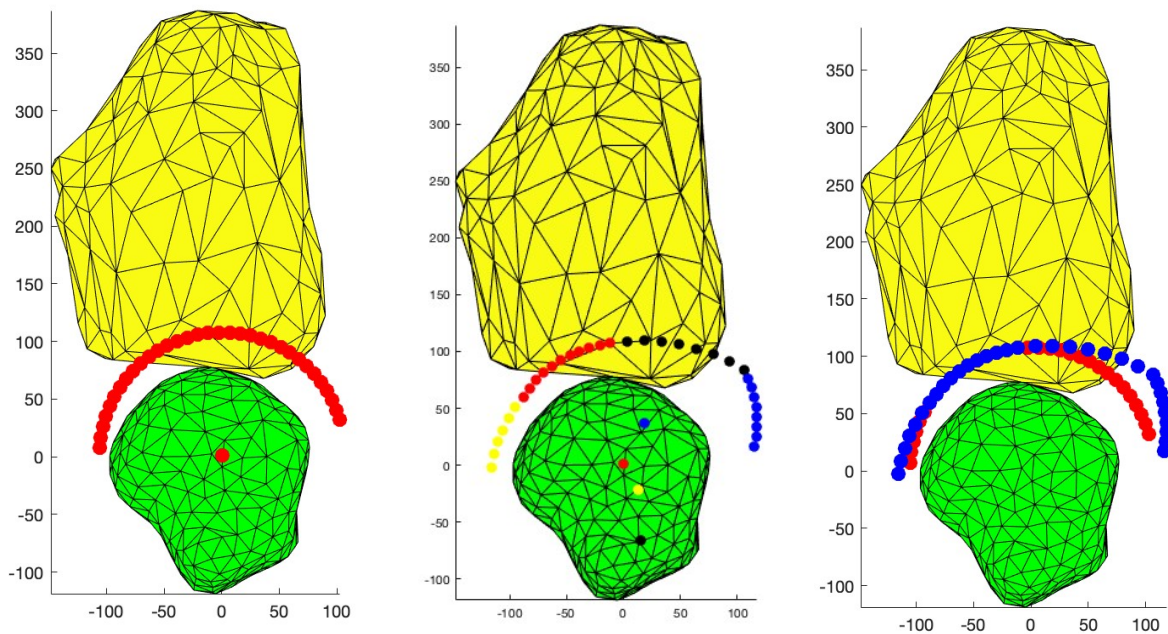


Fig. 33 – (left) Trajectory of fixed axis rotation, (middle) general motion and (right) the comparison

It is possible to see in the Fig. 33 that the general motion trajectory causes more free motion than the single axis rotation, this results in more tolerant motion to the deformity.

In the Fig. 34 is displayed a dependency of trajectory radius on ROM of forearm. The radius is increasing from the full supination to 40° of pronation, afterwards the radius is decreased in the full pronation. The red curve in the Fig. 34 is just the expectation, analytical expression has not been proven because of the lack of the data to be examined.

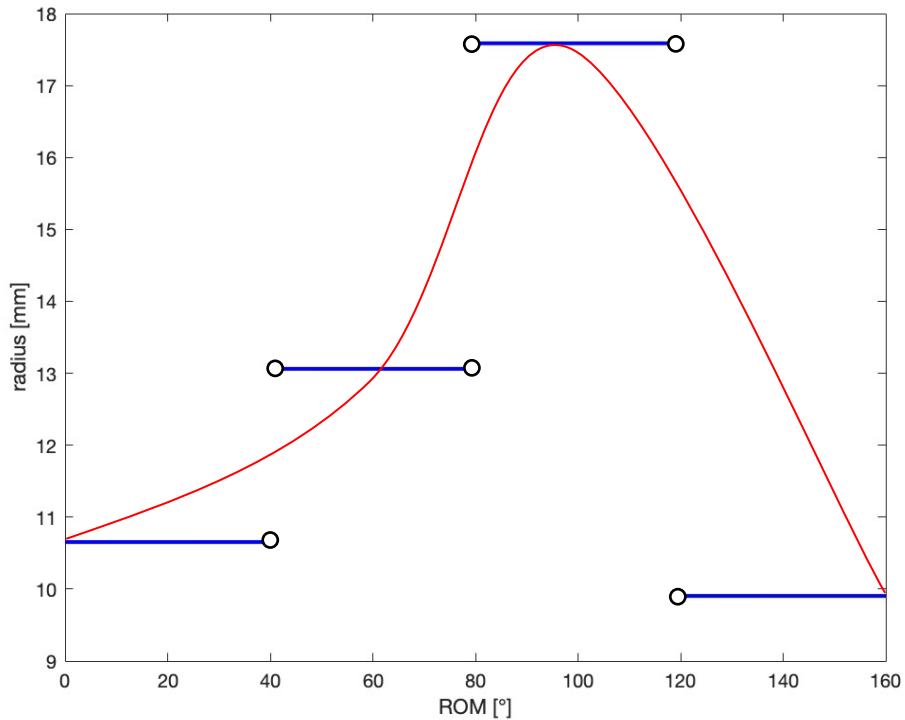


Fig. 34 – The dependency of trajectory radius on ROM of the forearm, with the expected shape of the curve (red)

5.2. PATHOLOGICAL ROTATION

The kinematics of forearm is significantly changing during the pathological rotation. A deformity of forearm bone introduces pathological mechanisms into the process that cannot be neglected. The results compare kinematics with and without these mechanisms. The theory is to converge to real pro/supination movement during the pathological rotation with increasing level of iteration. All can be verified by the clinical data with corresponding ROMs.

For demonstration in the results, patient 7 was chosen from the Tab. 1. To show the behavior of forearm kinematics in various ways of simulation from the most basic to the most complex.

5.2.1. KINEMATICS OF FREE ROTATION

The kinematics is neglecting all surrounding structure involved in the forearm complex. So, radius rotates around ulna with defined dynamic axis of rotation.

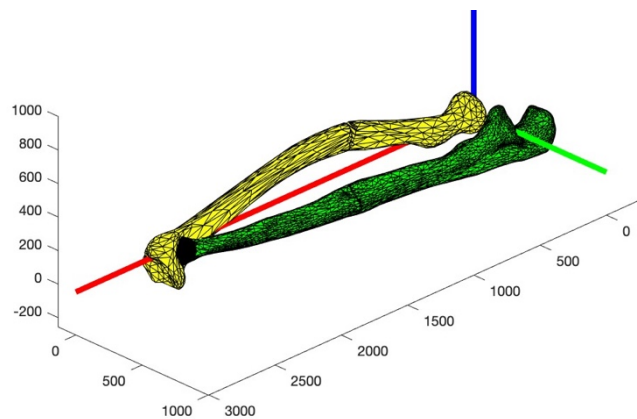


Fig. 35 – Initial bones configuration without surrounding structures

In the Fig. 35 it is possible to see that the patient wouldn't be able to hold the bones in the neutral position. This bones configuration is not possible. The bone surface intersection is too huge.

This is the example of a medial angulation that is 12° and it is located in the 40% of length of radius from the proximal end of radius. The reason why the configuration of the bones is unrealistic is that the angulation is relatively markable and the location of the angulation is in the proximal part of radius. Especially, the angulations in the proximal part have a big impact on the position of the end effector of the radius.

Therefore, the smaller deformities were examined in the interval $\langle 0^\circ, 1^\circ \rangle$ for the same patient.

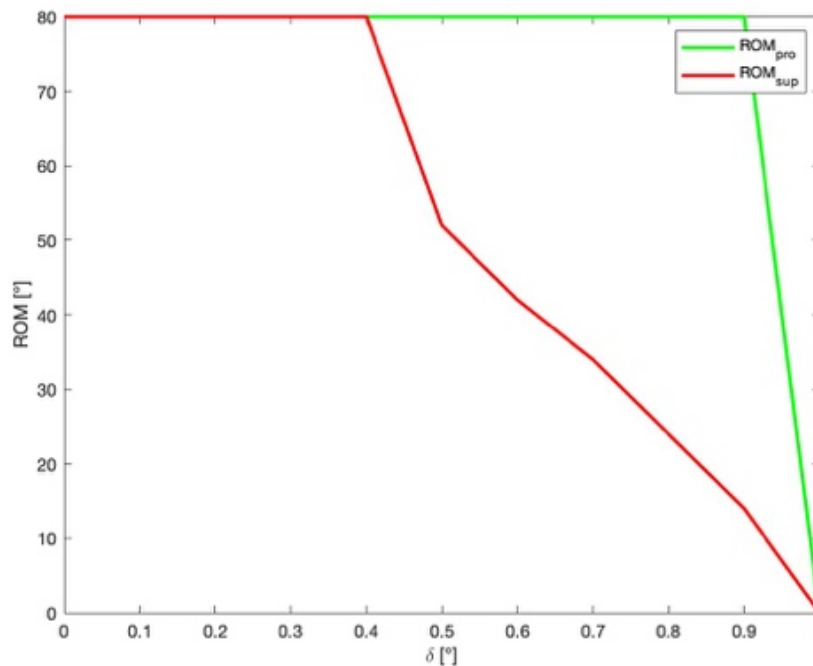


Fig. 36 – Dependency of ROM on the medial angulation angle δ – effect of soft tissues is not considered

In the Fig. 36 it is markable that the deformity 1° by medial angulation is enough to eliminate the ROM with considering just the bone kinematics without any influencing factors. The medial deformity 0.4° stills acceptable because the ROM is not affected at all. Even the angulation 0.5 is considered as not sever. The ROM is 130° in this case. In the Fig. 36 it is also visible that the ROM in pronation is more resistant to a deformity than in supination.

5.2.2. KINEMATICS –ROTATATION CENTRE TRANSLATION

In the first iteration the dislocation of axis of rotation was defined, caused by the kinematics of own deformity. Change of the ROM is observed. So, the effect of deformity kinematics is involved but without consideration of other forearm structures participating in the pathological kinematics. In the other words the translation of the centers of the rotation is not restricted and it is simulating the case when IOM and TFCC would be absolutely neglected. Because of this fact the initial configuration is unreal. The radius is fully intersecting the ulna – Fig. 35. This iteration affects just the kinematics but it doesn't affect the statical configuration in statical neutral position. That's why the rotation is not possible.

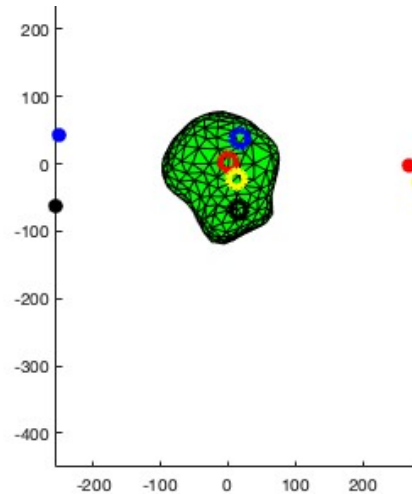


Fig. 37 – Translation of centers of rotation by own deformity, circles stand for original position of the centers of rotation and full points stand for translated centers of rotation.

In the Fig. 37 the original centers of rotation are marked with a colorful circle and the translated centers of rotation are marked with colorful point. This translation is caused by the deformity kinematics.

As already mentioned, this iteration does not affect the anatomical position in the neutral position, and thus rotation is not possible. Therefore, the behavior of this iteration for small deformations is presented as in the case when no pathological mechanical effects were considered.

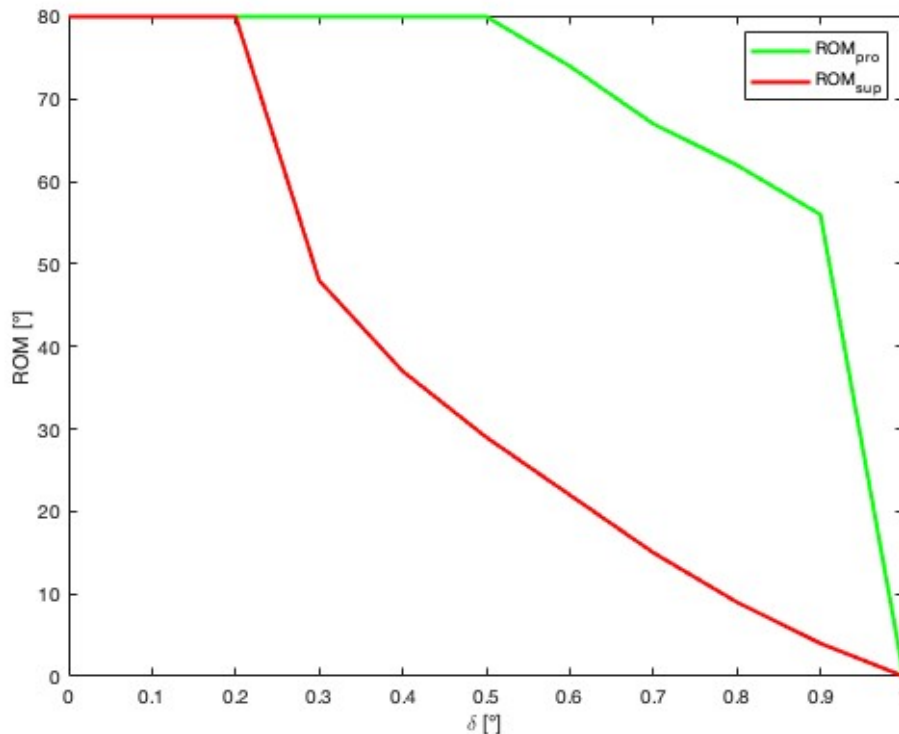


Fig. 38 – Dependency of ROM on the medial angulation angle δ – translation of the centers of rotation is considered

The dependency of ROM on the medial angulation angle (Fig. 38) shows that angulation 1° means the intersection in the neutral position, so afterwards no more motion is possible like in

the previous case. Because of the translation of the centers of rotation the ROM is more restricted with the increasing angulation. Full ROM can be hold till the medial angulation is 0.2° with consideration of this factor. In the previous case it was in comparison twice as much as with the first iteration. But it still be a problem with bigger angulations than 1° .

5.2.3. KINEMATICS – RADIOHUMERAL ROTATION

In the previous cases that there is a problem with bigger angulations than 1° , so it indicates that there must be another factor. This factor can be called the rotation in the radiohumeral junction. The stiffness of ligamentum anulare or stiffness of IOM is not considered. So, this pathological rotation is not restricted.

Now it could be seen in the Fig. 39 that the configuration of bones in the neutral position is anatomically possible. Actually, the starting neutral configuration seems to be very similar to the healthy configuration. In the case of patient 7 just medial angulation of radius is present that's why the theoretical adjustment is so precise without any contribution of surrounding forearm structures.

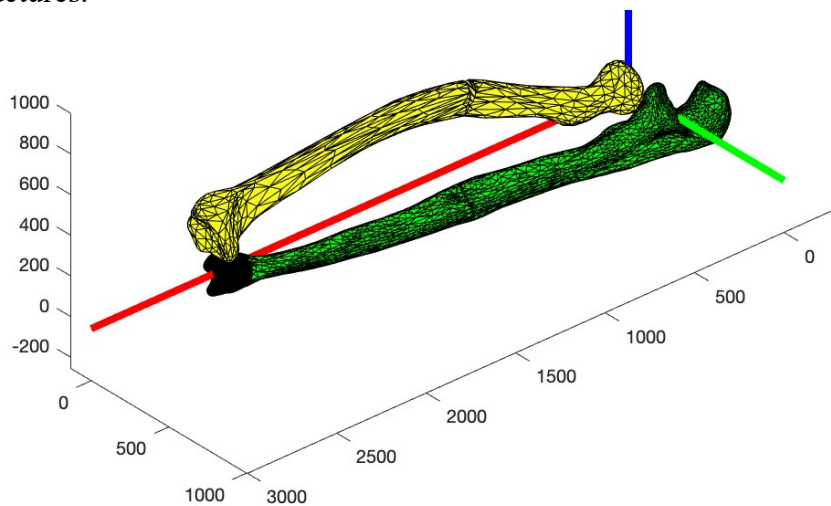


Fig. 39 – Configuration in neutral position wit considering the rotation in radiohumeral junction

The most import is how will the kinematics after this iteration look like. Firstly, let's display just the second iteration without the first (Fig 40 – left). Secondly, the first iteration was added into the algorithm (Fig 40 – right). The results are significantly different.

The kinematics without the first iteration involved exhibits full ROM whereas the kinematics with the first iteration doesn't any anatomically possible movement. The ROM is equal to zero.

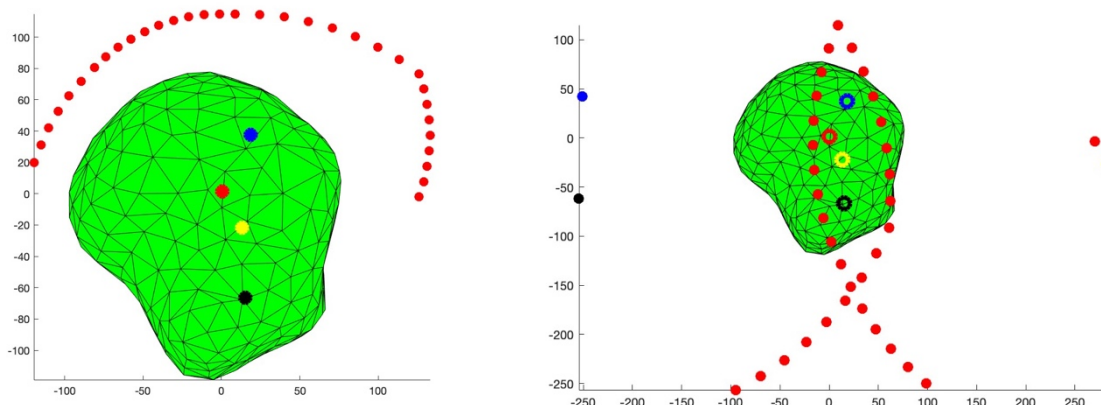


Fig. 40 – (left) The kinematics of radius considering just second iteraton and (right) combination of the first and the the second iteration

In reality the patient with this malunion had restricted both movements pronation and supination but he or she was able to rotate a little bit in both directions. ROM was 10-0-45. So, it means that there will be effect of both iterations, because anatomically correct configuration in neutral position was achieved with the second iteration and pro/supination movement was restricted with the first iteration.

From these results it is possible to see that there will be variable effect of surrounding forearm structures that cannot be neglected.

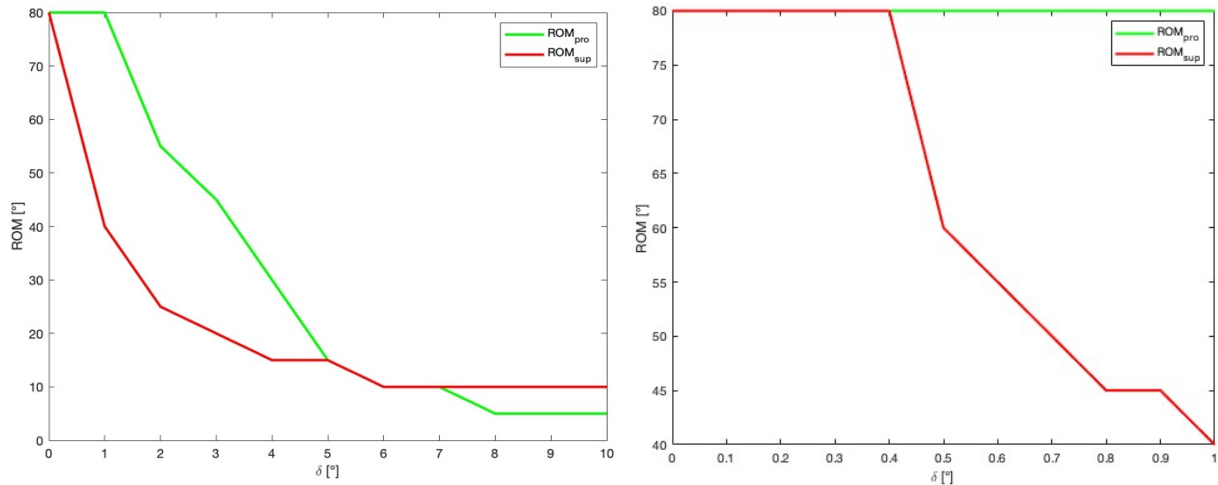


Fig. 41 – Dependency of ROM on the medial angulation angle δ – translation of the centers of rotation by own deformity and radiohumeral rotation are considered

The same dependencies as were done in previous iteration was done for the second iteration (Fig. 41). The Fig. 41 shows on the left the deformity in the interval $\delta \in < 0^\circ; 10^\circ >$ and on the right $\delta \in < 0^\circ; 1^\circ >$. Moreover, from the first iteration the ROM was possible to examine in the case of bigger deformities (to medial angulation 10°). In the Fig. 41 on right the pronation is not affected in the interval of small deformities. But supination is very sensitive even to medial malunion 0.5° . In the Fig. 41 on the left is visible that ROM in supination is decreasing faster than the ROM in pronation. Due to combination of the first and the second iteration more realistic forearm behavior is achieved.

These characteristics were done with combination of the first and the second iteration. So, the centers of rotation were translating according to deformity with increasing rotation angle in radiohumeral junction.

5.2.4. KINEMATICS – EFFECT OF STIFFNESS PARAMETRES

The third iteration is the last step to obtain the most relevant results of ROM from virtual modeling of forearm kinematics. Now, the four parameters are involved to estimate the effect of ligaments, soft tissues and muscles. For the determination of the parameters, SA optimization process was used. Cost function must be defined according to chapter 4.5.3:

$$CF: \min \left\{ (ROM_{pro} - 45^\circ)^2 + (ROM_{sup} - 10^\circ)^2 \right\}$$

This optimization was divided into the two parts. In the first we optimized four parameters. But the optimization took lots of time and the cost function decreased on value 625. The aim is to reach the value in the interval CF: $< 0; 50 >$. The worst case is 5° deviation from real value in supination and pronation as well.

The first optimization:

k_1	k_2	k_3	k_4
0,9945	0,1244	0,3477	0,5384

Tab. 2 – Obtained parameters after the first optimization process – meaning of the parameters is defined in the chapter 4.5.3

$$ROM_{pro} = 15^\circ ; ROM_{sup} = 15^\circ$$

From the table could be recognized that k_1 is converging to upper bound 1 and k_2 is converging to lower bound 0. It means that radius is fully rotated around mediolateral axis and around transvers axis it is not rotated at all. Therefore, an assumption was made for next optimization and it was set k_1 equal to 1 and k_2 equal to 0.

The second optimization:

k_1	k_2	k_3	k_4
1	0	0,4646	0,2340

Tab. 3 – Obtained parameters after the second optimization process – meaning of the parameters is defined in the chapter 4.5.3

$$ROM_{pro} = 45^\circ ; ROM_{sup} = 10^\circ$$

For the second optimization was enough 55 iterations to converge to cost function value equal to zero. Just two parameters were optimized, exactly the stiffness of DRUJ and distal part of IOM was adjusted. After estimation of the parameters, the simulation of the precise movement is possible in the case of the patient 7 with the concrete malunion.

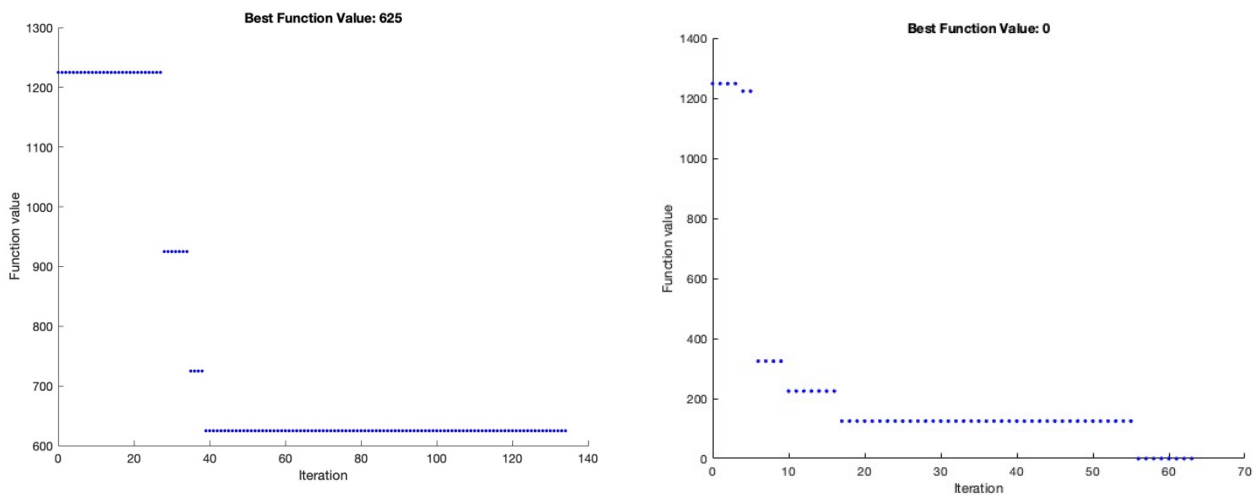


Fig. 42 – (left) The dependency of cost function value on iterations, the first optimization and (right) the second optimization

In the Fig. 43 there are displayed final positions in pronation and supination. Supination is almost entirely limited.

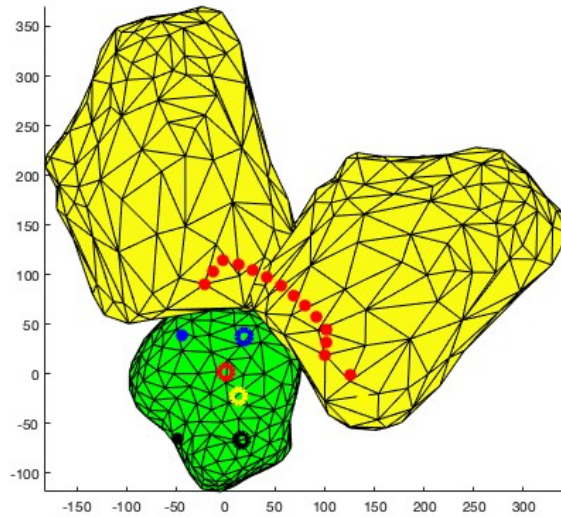


Fig. 43 – Simulation of the proper kinematics of the patient 7

In the order to know how each parameter is affecting the cost function value, the sensitivity analysis was done (Fig. 44).

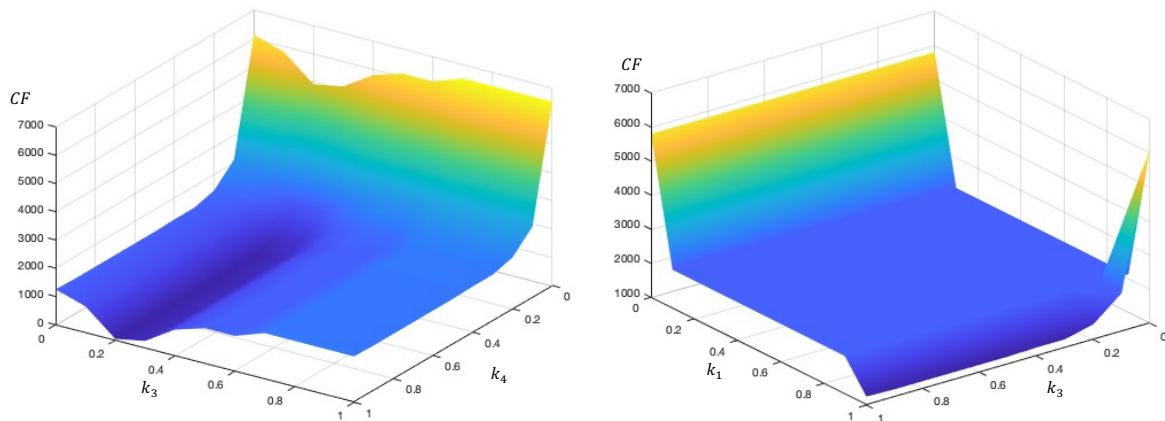


Fig. 44 – Sensitivity analysis for patient 7

The pairs of parameters were combined and changed. From the combination of k_3 and k_4 (Fig. 44 – left) it is possible to see that for minimizing CF the parameter k_3 doesn't have to change much but all it depends on the parameter k_4 . The second combination of k_3 and k_1 exhibits that k_1 must be equal to 1 and once again it doesn't depend on k_3 in the interval $\langle 0,3;1 \rangle$.

5.2.5. KINEMATICAL MODEL VERIFICATION

Our kinematical model was verified by a study that is listed in the Tab. 1. We are able to simulate arbitrary malunion of both bones. For the verification was used a dependency of ROM on the location of the malunion from the PRUJ. For set up of our model were used four parameters k_1, k_2, k_3, k_4 . The aim was to predict with our model the same results of ROM as the clinical observation.

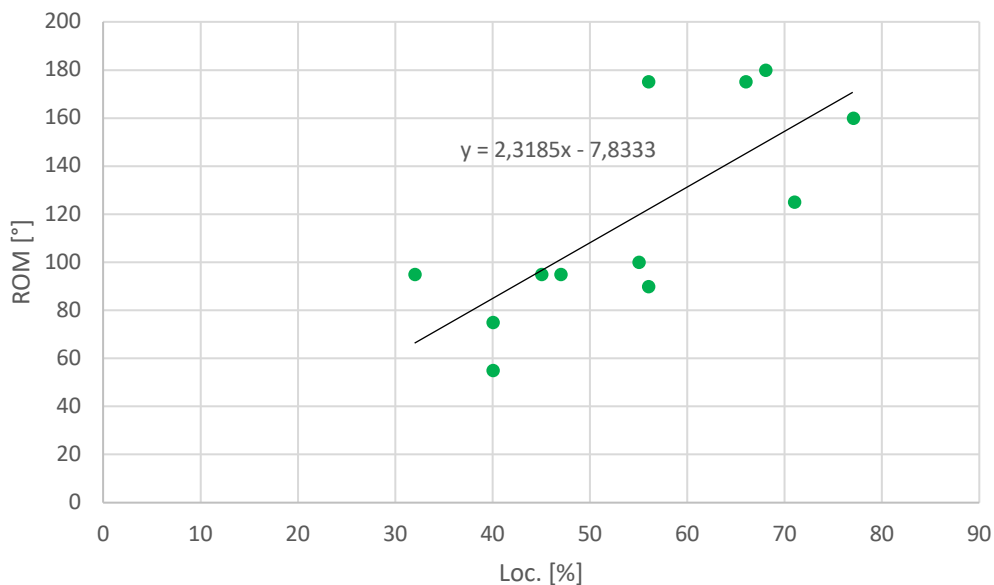


Fig. 46 – Clinical results measured in the study [12] – The dependency of ROM on malunion location

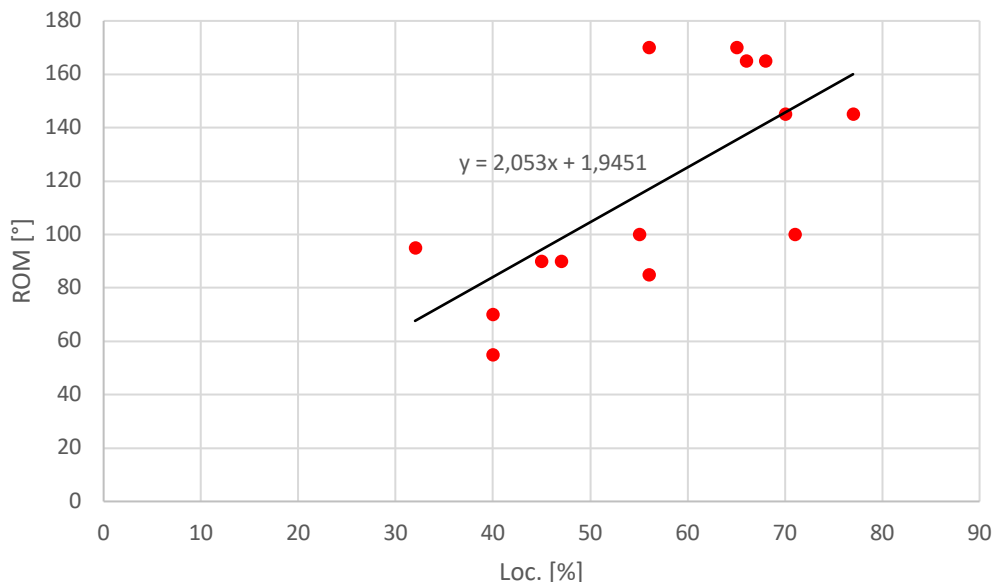


Fig. 45 – Simulated results by our model in accordance with study [12] – The dependency of ROM on malunion location

With our model the same dependency as the clinical results stated was predicted. Statistically could be said that ROM is decreasing with decreasing location of the malunion from the PRUJ. The severity of the malunion is increasing with the decreasing location from the PRUJ. This can be mathematically expressed by the linear dependency.

Data		Parameters				Mobility		
Patient	Loc [%]					Pronation	Supination	ROM
Number	-	k_1	k_2	k_3	k_4	[°]	[°]	[°]
1	47	1	0,1	0,1	0,1	15	75	90
3	56	1,23	20	0	0,3	10	75	85
4	32	0,5	0,6	0	0,5	5	90	95
5	71	0,25	4	0,08	0,35	40	60	100
6	45	0,7	0,5	0,05	0,16	20	70	90
7	40	1	0	0,46	0,23	45	10	55
8	40	0,75	5	0,5	0,07	70	0	70
9	55	0,85	0,5	0,33	0	90	10	100
11	56	0,85	0,2	0	0,27	70	100	170
12	66	0,65	0	0	1	70	95	165
13	77	0,88	0,63	0	0,3	75	70	145
14	68	0,6	0,8	0	1	65	100	165
15	70	0,3	0	0	0,16	65	80	145
17	65	0,67	0	0	0	80	90	170

Tab. 4 – Parameters set up for each patient according to study [12]

The parameters don't exhibit a dependency that could be interpreted. The parameters are random at all. Only it could be said that patient with full supination had parameter k_3 equal to zero. Normally the parameters are within the interval $\langle 0;1 \rangle$. In the table there are two patients that have parameter k_1 or k_2 greater than 1. Relatively complicated angulation of the ulna is the reason. In order to set up the radius into the proper configuration in the neutral position it is unavoidable to set a greater value of these parameters than is standardly selected.

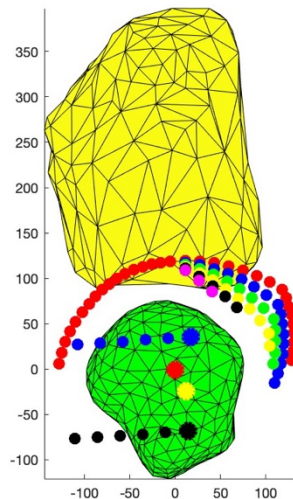


Fig. 47 – Stiffness of DRUJ in pronation

k_4	ROM_{pro} [°]
0	80
0,1	80
0,2	55
0,3	40
0,4	20
0,5	10

Tab. 5 – Stiffness of DRUJ in pronation

In the Fig. 47 is the patient 15. There is demonstrated an effect of the parameter k_4 symbolizing the compliance of DRUJ in the pronation. With the increasing stiffness of DRUJ in pronation, the parameter k_4 is increasing, the ROM is rapidly decreasing. It means that the effect of translation of the center of rotation by own deformity is increasing, so radius of rotation is increasing as well.

5.2.6. CLINICAL DATA EVALUATION

The data from the chapter 4.6. were used. ROM of both forearms was analyzed. The right forearm showed no signs of restricted rotation, while the left forearm had severely limited rotation. Therefore, was done the mirroring of left radius and ulna to right radius and ulna. From the mirroring it seems that ulna is not malunited there are some anatomical differences but no significant angulation was observed. Only left radius has volar angulation 8° . It can be also classified as a green stick fracture that is very common by children.

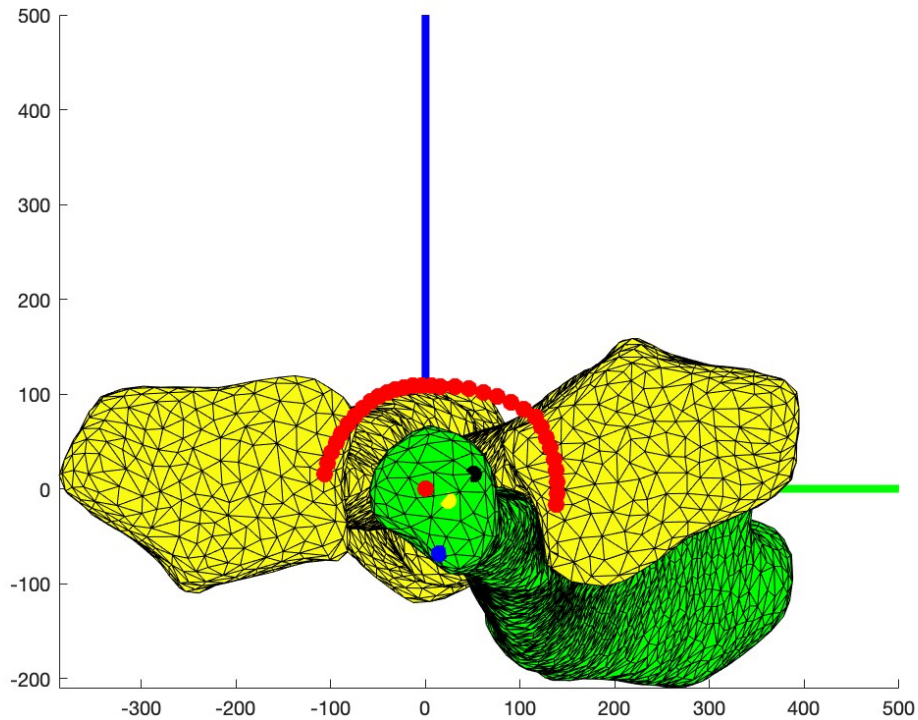


Fig. 48 – Right forearm analysis of ROM

ROM for right forearm rotation was examined: $80 - 0 - 75$ (Fig. 48). 75° in pronation is a limit value but it still acceptable for full ROM [15]. Pronation is anatomically limited because of a small protrusion located on the ulna, could be seen in the Fig. 49.

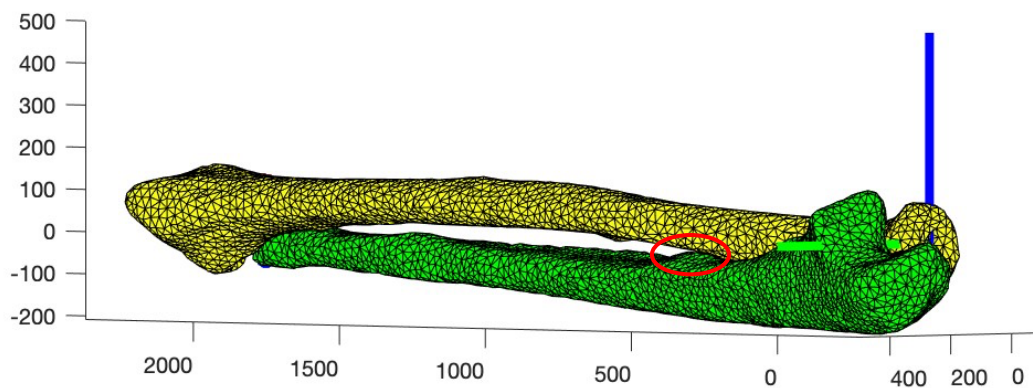


Fig. 49 – Limitation of the pronation

Left forearm had ROM (Fig. 50): 80 – 0 – 50 in the case of considering the effect of translated centers of rotation by the angulation and structures: TFCC and distal IOM. The contact was observed in the proximal part of the ulna and radius. The compliance of TFCC and distal IOM was reduced by 50%. The supination is not restricted.

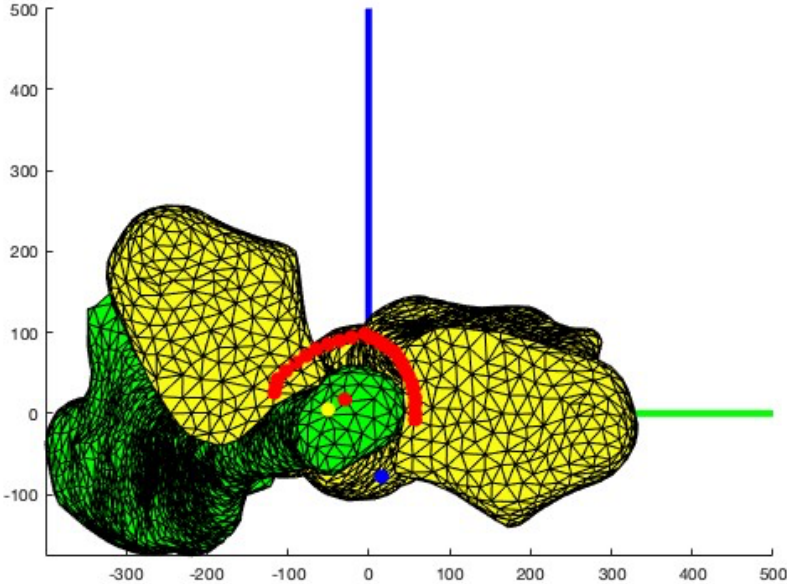


Fig. 50 – Patien radius trajectory computation

The case when the compliance of TFCC and distal IOM is reduced by 100% was also simulated, so the DRUJ is absolutely stiff (Fig. 51). In this case is the contact observed between the articulating surfaces of DRUJ. The ROM is 25 – 0 – 25, practically the patient would not be able to rotate with the hand.

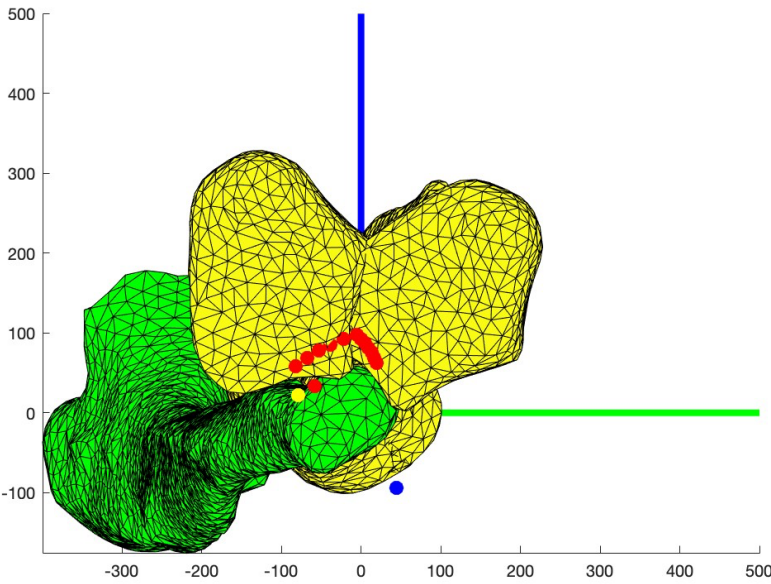


Fig. 51 – Fully restricted motion of the patient forearm, the DRUJ is absolutely stiff

Lastly, the simulation was done where the translation of the centers of rotation due to angulation is neglected, in the other words the DRUJ would be absolutely compliant.

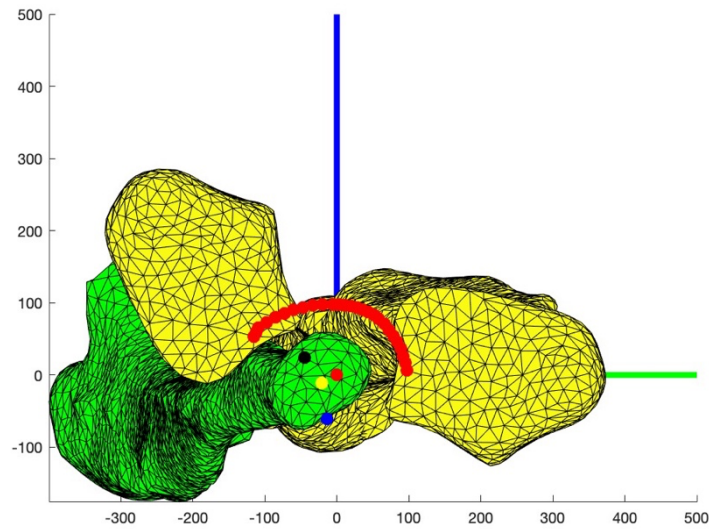


Fig. 52 – Fully free motion of the patient forearm, the DRUJ is absolutely compliant

In this case the ROM is the same as in the first case, so it is 80 – 0 – 50. Generally speaking, if the compliance of DRUJ is restricted by more than by 50% the ROM is going to decrease but till 50% it will be unchangeable. The contact will remain in the proximal part of the bones. That is predictable in the case of such a patient as we have. The children have compliant joints but if the deformity causes contact of the bones in the proximal or the middle part, the restriction of the ROM can't be eliminated by the increasing compliance.

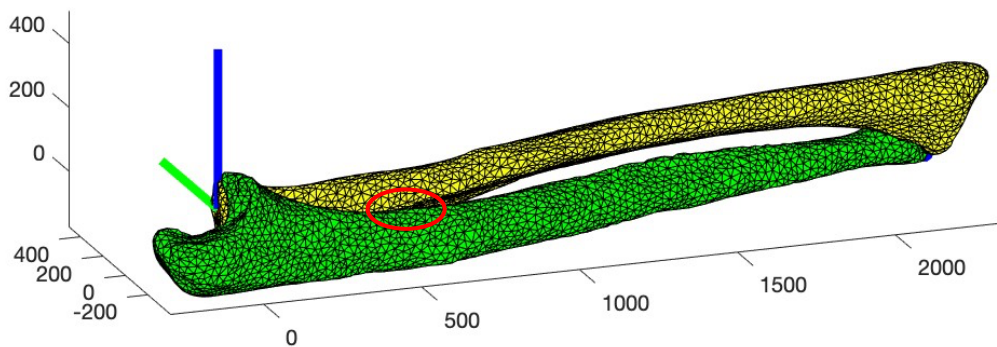


Fig. 53 – Protusion on the ulna, that limits the ROM in pronation

6. DISCUSSION

Two methods were realized for modeling forearm pro/supination movement. Firstly, attention was devoted to normal rotation and secondly, pathological rotation was described. All methods include new approaches that are based on the biomechanics of surrounding forearm structures. For the normal rotation was assumed just simple rotation round single axis of rotation. The results show that this rotation would be anatomically possible. No contact was observed, if the end effector of the axis of rotation was placed in the proper position. This fact comes to the discussion. Practically it is not possible to accurately state the axis of rotation. It is just known that it goes from the head of radius to the head of ulna. But coordinates position is unknown. The reason is that it will vary for different individuals. The geometry of the bones is individual and also the configuration of soft tissues, muscles and ligaments. Also, the maximal ROM varies because of the previous mentioned facts. That's why only way how to determine the axis of rotation is to rotate the radius around the ulna and observe when no contact is observed. Based on this method it is possible to determine a set of the acceptable vectors that satisfy this condition. So, it is not possible to determine the accurate position of axis of rotation with this method but the approximate position can be estimated.

Solving the dynamic center of rotation, the reality could be described more precisely due to cadaver forearm rotation. This study demonstrated more complex trajectory of the movement than is the simple circle as was assumed. There was found a new approach to determine the trajectory of pro/supination movement based on the study of forearm cadaver motion. Due to this study the geometry of bones was considered that's why the movement is more realistic. On the other hand, it was a cadaver test where the surrounding structures don't have the real material properties and radius is not driven by functional muscle system. Moreover, the scaling was done to transfer the results from cadaver to our virtual model. With this step, we also commit positional inaccuracy, which subsequently affects the trajectory of the movement. The entire trajectory of pronation is also not known from the cadaver study, basically the last position of the center of rotation is missing. In order to determine this position last center of rotation was estimated based on the mechanics of TFCC.

To conclude the estimated trajectory during normal rotation, it just converges to real trajectory that surely differ for each individual. To determine the exact trajectory of each individual, a sequence of x-rays in continuous motion would have to be performed by a healthy patient, which is impossible to the health risks the individual would be expose to.

The forearm model of the pathological rotation was verified in accordance with the study [12]. Malunion models were made for individual patients. Just single forearm bones 3D model was used for this verification. First thing that comes to the discussion is a fact that all simulated malunions were done on the same bone geometry. It is known that the geometry of ulna and radius is individual and it can significantly influence the pro/supination trajectory. For example, the location of the malunions was defined by a percentage distance from PRUJ. The fact is that the length of bones is different for each patient. So, it is not possible to precisely located the malunion. The malunions can grow to the length that is also a fact which is not considered.

Four factors were listed that are involved in pathological rotation. The first iteration is considering a fact that the centers of rotation are translated due to angulation. This mechanism is listed in the study [10] and it was implemented into our model. The precise mechanism of this translation is unknown. It is just our hypothesis that definition of the translation vector is the same as is the vector that defines the angulation. Otherwise, it is not known accurately the magnitude of translation vectors in the reality.

The second iteration helps us to simulate properly the angulated configuration in the neutral position. This mechanism must function due to compliance of the soft tissues, muscle and ligaments. Only way how to get a reasonable configuration in the neutral position is to rotate

the radius in a radiohumeral joint around two axes. Although this fact is well known, the exact magnitude of this pathological rotation is not known. Just the estimate was done.

The third iteration should optimize the previous two iterations in order to get final estimation of the trajectory. This iteration reacts on the studies [12, 13, 17]. The solidification mechanism of IOM is explained in the Fig. 25 – [12]. This solidification of ligaments has an effect on the pro/supination. According to study [13] the presence of TFCC has an effect on the contact area therefore also an effect on the stiffness of DRUJ. It was confirmed in the Fig. 47. The laxity of the radial head in PRUJ was involved in our model according to studies [15, 16]. This is handled using constants k_1 and k_2 . Set up of the values of the parameters should be in the range between 0 and 1. But in the case of complicated malunion where are both bones involved with sever angulations the value of k_1 or k_2 can exceed 1. This can be done precisely if the ROM of the patient is known. In the opposite case the values must be just estimated based on the age for example. The age affects the stiffness of the PRUJ and DRUJ.

The fourth iteration is just an assumption how to deal with the longitudinal radius translation, the rection on the study [14]. This phenomenon is sometimes observed when a fracture or malunion occurs. The radius is also translated in the longitudinal direction during the normal rotation. But it is unknow how much it can be translated. That's one of the reasons why this factor wasn't implemented into our model. Also, in the table is not specified if the radius was translated or not. So, it can't be verified. It would also make our model more sophisticated and it would bring into our model more mistakes and instability.

Our model verified the fact, that comes from studies [11, 12], the pronation can maintain therefore, it is not so prone to deformity. This could be seen in the Fig. 41.

We have laid the foundations for the expansion of modern 3D preoperative planning methods. Our innovative approach took into account pre- and post-operative kinematics, which current 3D planning software lacks. Our mathematical description of forearm kinematics may be used in other new versions of medical software in the future.

Thanks to our contribution, it would be possible to decide whether to use 3D printed custom restorations, or to use a conventional operation procedure, where the small imperceptions could be left. Nowadays the 3D preoperative softwares use just the mirroring of the forearm bones to examine the deformity. The anatomical differences could be found between the right and left bone. This could lead to wrong osteotomy planning and it may cause an imperfection in the forearm alignment. Our model brings contrary the control by post operative kinematics if the osteotomy planning is fully correct. This introduces more precise 3D planning.

In addition, the amount that the insurance company must pay for a conventional operation is 40,000 CZK. A cost of 100,000 CZK must be paid for an operation with 3D planning, 3D printing of special splints, and guide bushings. [27] Our model is able to decide if the operation using 3D printing is necessary or not. This can save lots of money spent on reoperations. Our model uses the individual geometry from CT data. Individual geometry of the bones has an influence on post operative ROM that can be simulated by our model.

CONCLUSIONS

Within the presented study we have developed a simulation model that predict pronation/supination trajectory in both normal and pathological conditions. In contrary to previous studies that consider fixed rotation axis of the radius around the ulna, we have shown that the center of rotation of distal radioulnar joint follows complex movement. We have further shown that pronation and supination is to a great extent influenced by the contribution of the soft structures. Our model allows to simulate kinematics of forearm with deformity and thereby accurately simulate the clinically detected pathological conditions of pro/supination in different patients.

We have verified a hypothesis that a small deformity can influence the ROM significantly. Therefore, we recommend preoperative planning with considering complex kinematics. The second hypothesis that distal radioulnar joint stiffness influences ROM significantly was also confirmed in simulation. The mathematical analysis indicates the need to include ligaments and soft tissues into the kinematical model. Finally, our model was applied to a real forearm malunions. We have shown that forearm kinematics is more complex than was previously assumed that makes surgery in the forearm region challenging. Our research provides a theoretical basis for improvement of preoperative planning software without the need to mirror contralateral hand.

REFERENCES

- [1] – DUMONTIER, Christian and Marc SOUBEYRAND. *European Surgical Orthopaedics and Traumatology: The EFORT Textbook*. Springer, 2014. ISBN 978-3-642-34746-7.
- [2] – PILNÝ, Jaroslav, Roman SLODIČKA and et al. *Chirurgie ruky*. 2. Grada, 2017. ISBN 978-80-271-0180-1.
- [3] – Tsitsilonis S, Machó D, Manegold S, Krapohl BD, Wichlas F. *Fracture severity of distal radius fractures treated with locking plating correlates with limitations in ulnar abduction and inferior health-related quality of life*. GMS Interdiscip Plast Reconstr Surg DGPW. 2016 Jul 28;5: Doc20. doi: 10.3205/iprs000099. PMID: 27547692; PMCID: PMC4977376.
- [4] – FORMALSKI, Stefan, Ranjan GUPTA and Thay Q. LEE. Anatomy and Biomechanics of the Elbow Joint. *Techniques in Hand and Upper Extremity Surgery*. 2003, 168–178.
- [5] – JONES, Oliver (2020) *The Radioulnar joints*. TeachMeAnatomy. [online]. Copyright © [cit. 02.08.2022]. Available from: <https://teachmeanatomy.info/upper-limb/joints/radioulnar-joints/>
- [6] – Lees VC. *The functional anatomy of forearm rotation*. J Hand Microsurg. 2009 Dec;1(2):92-9. doi: 10.1007/s12593-009-0022-7. Epub 2010 Jan 8. PMID: 23129940; PMCID: PMC3453027.
- [7] – Wijffels M, Brink P, Schipper I. *Clinical and non-clinical aspects of distal radioulnar joint instability*. Open Orthop J. 2012; 6:204-10. doi: 10.2174/1874325001206010204. Epub 2012 May 30. PMID: 22675411; PMCID: PMC3367466.
- [8] – Adams JE. *Forearm Instability: Anatomy, Biomechanics, and Treatment Options*. J Hand Surg Am. 2017 Jan;42(1):47-52. doi: 10.1016/j.jhsa.2016.10.017. PMID: 28052828.
- [9] – Mitchell B, Whited L. Anatomy, Shoulder and Upper Limb, Forearm Muscles. 2022 Jun 14. In: StatPearls [internet]. Treasure Island (FL): StatPearls Publishing; 2022 Jan–. PMID: 30725660.
- [10] – KATT, Brian, Daniel SEIGERMAN, Kevin LUTSKY and Pedro BEREDJIKLIJAN. Distal Radius Malunion. *The Journal of Hand Surgery*. 2020, 168–178. Available from: <https://doi.org/10.1016/j.jhsa.2020.02.008>
- [11] – Jeuken RM, Hendrickx RPM, Schotanus MGM, Jansen EJ. *Near-anatomical correction using a CT-guided technique of a forearm malunion in a 15-year-old girl: A case report including surgical technique*. Orthop Traumatol Surg Res. 2017 Sep;103(5):783-790. doi: 10.1016/j.otsr.2017.03.017. Epub 2017 Apr 17. PMID: 28428034.
- [12] – Nagy L, Jankauskas L, Dumont CE. *Correction of forearm malunion guided by the preoperative complaint*. Clin Orthop Relat Res. 2008 Jun;466(6):1419-28. doi: 10.1007/s11999-008-0234-3. Epub 2008 Apr 11. PMID: 18404294; PMCID: PMC2384037.

- [13] – Gammon B, Lalone E, Nishiwaki M, Willing R, Johnson J, King GJW. *The Effect of Dorsal Angulation on Distal Radioulnar Joint Arthrokinematics Measured Using Intercartilagous Distance*. J Wrist Surg. 2019 Feb;8(1):10-17. doi: 10.1055/s-0038-1667303. Epub 2018 Aug 15. PMID: 30723596; PMCID: PMC6358445.
- [14] – Rabinowitz RS, Light TR, Havey RM, Gourineni P, Patwardhan AG, Sartori MJ, Vrbos L. *The role of the interosseous membrane and triangular fibrocartilage complex in forearm stability*. J Hand Surg Am. 1994 May;19(3):385-93. doi: 10.1016/0363-5023(94)90050-7. PMID: 8056963.
- [15] – LaStayo PC, Lee MJ. *The forearm complex: anatomy, biomechanics and clinical considerations*. J Hand Ther. 2006 Apr-Jun;19(2):137-44. doi: 10.1197/j.jht.2006.02.002. PMID: 16713861.
- [16] – Tatebe M, Shinohara T, Okui N, Yamamoto M, Kurimoto S, Hirata H. *Tilt of the radius from forearm rotational axis reliably predicts rotational improvement after corrective osteotomy for malunited forearm fractures*. Nagoya J Med Sci. 2012 Feb;74(1-2):167-71. PMID: 22515123; PMCID: PMC4831262.
- [17] – Jayakumar P, Jupiter JB. *Reconstruction of malunited diaphyseal fractures of the forearm*. Hand (N Y). 2014 Sep;9(3):265-73. doi: 10.1007/s11552-014-9635-9. PMID: 25191155; PMCID: PMC4152429.
- [18] – Fedorov A, Beichel R, Kalpathy-Cramer J, Finet J, Fillion-Robin JC, Pujol S, Bauer C, Jennings D, Fennessy F, Sonka M, Buatti J, Aylward S, Miller JV, Pieper S, Kikinis R. *3D Slicer as an image computing platform for the Quantitative Imaging Network*. Magn Reson Imaging. 2012 Nov;30(9):1323-41. doi: 10.1016/j.mri.2012.05.001. Epub 2012 Jul 6. PMID: 22770690; PMCID: PMC3466397.
- [19] – Ružička P., Pehlivan E., Černý J. *Aditivní technologie v medicínských aplikacích*. Biomechanika III. 2105. CTU, Faculty of mechanical engineering
- [20] – MCGINTY, Bob. *Rotation Matrices*. *Continuum Mechanics* [online]. 2012 [cit. 2022-08-02]. Available from: <https://www.continuummechanics.org/rotationmatrix.html>
- [21] – LAB 3 Prelab: Solving over – determined systems using MATLAB, Rose-Hulman Institute of Technology [online]. Copyright ©u [cit. 29.07.2022]. Available from: <https://www.rose-hulman.edu/ES205/PDFs/lab-3-prelab.pdf>
- [22] – Jaroslaw Tuszynski (2022). *Surface Intersection*. (<https://www.mathworks.com/matlabcentral/fileexchange/48613-surface-intersection>), MATLAB Central File Exchange. Retrieved August 2, 2022.
- [23] – MÖLLER, Tomas. *A Fast Triangle – Triangle Intersection Test* [online]. 1997 [cit. 2022-08-02]. Available from: <https://web.stanford.edu/class/cs277/resources/papers/Moller1997b.pdf>. Stanford University.
- [24] – Xin-She Yang, Chapter 4 - *Simulated Annealing*, Editor(s): Xin-She Yang, Nature-Inspired Optimization Algorithms, Elsevier, 2014, Pages 67-75, ISBN 9780124167438, <https://doi.org/10.1016/B978-0-12-416743-8.00004-X>.

[25] – Yasutomi T, Nakatsuchi Y, Koike H. *Anterior dislocation of the radial head secondary to malunion of the forearm bones*. J Shoulder Elbow Surg. 2000 Nov-Dec;9(6):536-40. doi: 10.1067/mse.2000.109409. PMID: 11155310.

[26] – Kebrle Radek, Forearm cadaver kinematics, obtained from the communication.

[27] – *TÉMA: Pacienti mi ted' víc věří*. IX. Praha, Smíchov: MAFRA, 2022. ISSN 2336 – 4815.

LIST OF FIGURES

Fig. 1 – The elbow joint [4].....	8
Fig. 2 – Interosseous membrane [8]	9
Fig. 3 – PRUJ, ligamentum anulare [5].....	9
Fig. 4 – DRUJ, TFCC [7]	10
Fig. 5 – ROM investigation in the case of patients with forearm malunion [12].....	12
Fig. 6 – Radial tilt [16]	15
Fig. 7 – 3D Slicer, segmentation options	18
Fig. 8 – (left) Comparison of thresholding and (right) grow from seeds algorithm	18
Fig. 9 – 3D Slicer procedure schema	19
Fig. 10 – STL reconstruction procedure to MATLAB.....	19
Fig. 11 – CT scans processing schema.....	20
Fig. 12 – Triangle – Triangle intersection test [23].....	22
Fig. 13 – Definition of new coordinate system	23
Fig. 14 – Least Squares Method defining dynamic center of rotation	26
Fig. 15 – (left) Radius measurement in Tracker and (right) in MATLAB.....	26
Fig. 16 – Usage of anatomical landmarks to define center of rotation	27
Fig. 17 – Vectors defining the kinematic of malunion.....	28
Fig. 18 – Definition of angulation plane by angle β and angle δ responsible for axial angulation	28
Fig. 19 – Malunion reconstruction – CT scans [25] to MATLAB angulated forearm model.	31
Fig. 20 – Vector translation of center of rotation by the angulation of radius	31
Fig. 21 – Composition of the translation vector due to radius and ulna malunion	32
Fig. 22 – The direction of the vector Δ	32
Fig. 23 – Geometry for an estimate of radiohumeral rotation.....	33
Fig. 24 – (left) Exaggerated ventro – dorsal rotation and (right) exaggerated medio – lateral	33
Fig. 25 – Simplification of the IOM mechanics during the angulation of radius	34
Fig. 26 – Consideration of articulating surface for SA algorithm.....	36
Fig. 27 – SA scheme [24].....	36
Fig. 28 – CT scans reconstruction in the 3D Slicer to 3D model.....	38
Fig. 29 – (left) Mirroring of radius and (right) ulna in MATLAB.....	38
Fig. 30 – Definition of translation vector Δ	39
Fig. 31 – Initial vectors definition	39
Fig. 32 – Rotation algorithm schema	41
Fig. 33 – (left) Trajectory of fixed axis rotation, (middle) general motion and (right) the comparison	42
Fig. 34 – The dependency of trajectory radius on ROM of the forearm, with the expected shape of the curve (red).....	43
Fig. 35 – Initial bones configuration without surrounding structures	43
Fig. 36 – Dependency of ROM on the medial angulation angle δ – effect of soft tissues is not considered.....	44
Fig. 37 – Translation of centers of rotation by own deformity, circles stand for original position of the centers of rotation and full points stand for translated centers of rotation.....	45
Fig. 38 – Dependency of ROM on the medial angulation angle δ – translation of the centers of rotation is considered	45
Fig. 39 – Configuration in neutral position with considering the rotation in radiohumeral junction.....	46
Fig. 40 – The kinematics of radius considering just second iteration (left) and combination of the first and the second iteration (right)	46

Fig. 41 – Dependency of ROM on the medial angulation angle δ – translation of the centers of rotation by own deformity and radiohumeral rotation are considered.....	47
Fig. 42 – (left) The dependency of cost function value on iterations, the first optimization and (right) the second optimization.....	48
Fig. 43 – Simulation of the proper kinematics of the patient 7	49
Fig. 44 – Sensitivity analysis for patient 7	49
Fig. 45 – Simulated results by our model in accordance with study [12] – The dependency of ROM on malunion location.....	50
Fig. 46 – Clinical results measured in the study [12] – The dependency of ROM on malunion location	50
Fig. 47 – Stiffness of DRUJ in pronation.....	51
Fig. 48 – Right forearm analysis of ROM.....	52
Fig. 49 – Limitation of the pronation	52
Fig. 50 – Patien radius trajectory computation	53
Fig. 51 – Fully restricted motion of the patient forearm, the DRUJ is absolutely stiff.....	53
Fig. 52 – Fully free motion of the patient forearm, the DRUJ is absolutely compliant.....	54
Fig. 53 – Protursion on the ulna, that limits the ROM in pronation.....	54

LIST OF TABLES

Tab. 1 – Patients – Malunion definition and individual ROM [12]	30
Tab. 2 – Obtained parameters after the first optimalization process – meaning of the parameters is defined in the chapter 4.5.3	48
Tab. 3 – Obtained parameters after the second optimalization process – meaning of the parameters is defined in the chapter 4.5.3	48
Tab. 4 – Parameters set up for each patient according to study [12]	51
Tab. 5 – Stiffness of DRUJ in pronation	51